Journal of Scientific Computing (2023) 96:56
https://doi.org/10.1007/s10915-023-02281-8

New Low-Dissipation Central-Upwind Schemes

Alexander Kurganov[1] · **Ruixiao Xin**[1]

Received: 10 October 2022 / Revised: 16 June 2023 / Accepted: 17 June 2023 /
Published online: 4 July 2023

Abstract
In this paper, we develop new second-order low-dissipation central-upwind (LDCU) schemes for hyperbolic systems of conservation laws. Like all of the Godunov-type schemes, the proposed LDCU schemes are developed in three steps: reconstruction, evolution, and projection. A major novelty of our approach is in the projection step, which is based on a subcell resolution and designed to sharper approximate contact waves while ensuring a non-oscillatory property of the projected solution. In order to achieve this goal, we take into account properties of the contact waves. We design the LDCU schemes for both the one- and two-dimensional Euler equations of gas dynamics. The new schemes are tested on a variety of numerical examples. The obtained results clearly demonstrate that the proposed LDCU schemes contain substantially smaller amount of numerical dissipation and achieve higher resolution compared with their existing counterparts.

Keywords Hyperbolic systems of conservation laws · Low-dissipation central-upwind schemes · Subcell resolution · Contact discontinuities · Euler equations of gas dynamics

Mathematics Subject Classification 76M12 · 65M08 · 76N15 · 35L65 · 35L67

1 Introduction

We focus on the development of high-resolution finite-volume schemes for hyperbolic systems of conservation laws. We consider one-dimensional (1-D),

$$\boldsymbol{U}_t + \boldsymbol{F}(\boldsymbol{U})_x = \boldsymbol{0}, \tag{1.1}$$

and two-dimensional (2-D),

$$\boldsymbol{U}_t + \boldsymbol{F}(\boldsymbol{U})_x + \boldsymbol{G}(\boldsymbol{U})_y = \boldsymbol{0}, \tag{1.2}$$

✉ Alexander Kurganov
alexander@sustech.edu.cn

Ruixiao Xin
xinrx@mail.sustech.edu.cn

[1] Department of Mathematics, Shenzhen International Center for Mathematics and Guangdong Provincial Key Laboratory of Computational Science and Material Design, Southern University of Science and Technology, Shenzhen 518055, China

systems. Here, x and y are spatial variables, t is the time, $\boldsymbol{U} \in \mathbb{R}^d$ is a vector of unknowns, and $\boldsymbol{F}$ and $\boldsymbol{G}$ are the x- and y-directional fluxes.

Development of highly accurate and robust numerical methods for the hyperbolic systems of conservation laws is a quite challenging task as solutions of (1.1) and (1.2) may develop complicated structures including shock waves, contact discontinuities, rarefaction and shear zones, as well as their interactions. Finite-volume Godunov-type schemes for (1.1) and (1.2) are popular as they rely on the integral formulations of these systems, which better fit the definition of weak solutions to be numerically captured. In general, Godunov-type schemes are constructed as follows. Given the cell averages of the solution, first a piecewise polynomial approximation (needed to increase the accuracy of the resulting scheme) is constructed and then the solution is evolved to the next time level by integrating (1.1) or (1.2) over a set of space-time control volumes (CVs).

Depending on the way these CVs are selected, we may or may not need to solve the (generalized) Riemann problems in order to integrate the fluxes along the boundaries of the CVs. Solving (generalized) Riemann problems (either exactly or approximately) is required to develop upwind schemes, which are typically quite accurate as they take into account the properties of the exact solutions of (1.1) or (1.2). A drawback of upwind schemes, however, is in the fact that solving (generalized) Riemann problems may be hard, computationally expensive, or even impossible. In fact, most of the existing upwind schemes are developed for the 1-D system (1.1) and then extended to the multidimensional case in a "dimension-by-dimension" manner as (even approximately) solving 2-D Riemann problems is an extremely challenging task. Over years, a variety of upwind schemes have been developed; see, e.g., the monographs [3, 17, 33] and references therein.

Godunov-type central schemes provide a much simpler alternative to their upwind counterparts as they are based on the CVs selected in such a way (for example, using a staggered mesh) that solving (generalized) Riemann problems can be avoided. Instead, the flux integrals are approximated using appropriate quadratures: this is possible as in the central setting the fluxes are integrated over the smooth parts of the solution. This makes central schemes simple and easily applicable "black-box" solvers for a wide variety of hyperbolic systems (1.2). Staggered central schemes were first proposed in [24] and then further developed in [1, 2, 4, 9, 18–20, 23, 26] to name just a few.

A major drawback of Godunov-type central schemes, however, is their relatively large numerical dissipation, which might smear discontinuities and especially linearly degenerate contact waves. In order to reduce the amount of numerical dissipation present in central schemes, a new class of central-upwind (CU) schemes was proposed in [12, 15, 16]. The key idea behind the construction of the CU schemes for the 1-D system (1.1) is to select the CVs of the size proportional to the local speeds of propagation so that all of the nonlinear and potentially nonsmooth waves stay inside those "nonsmooth" CVs. In addition, "smooth" CVs are set between the "nonsmooth" ones and the solution is evolved (using the integral form of the system (1.2) without solving any (generalized) Riemann problems) in both of them. This leads to doubling the number of computed cell averages at the end of each time step. In order to develop a practically feasible scheme, at the end of each time step the evolved solution has to be projected back onto the original finite volume mesh. The projection should be carried out in a very careful manner as the projection step may bring an excessive amount of numerical dissipation into the resulting scheme as was the case in the original CU schemes introduced in [12, 15, 16]. In order to more accurately project the solution, we had used in [10] a sharper piecewise linear reconstruction of the evolved (intermediate) solution. This helped to reduce the amount of numerical dissipation, but the improvement in the resolution, especially in the resolution of linearly degenerate contact waves was rather minor. Another advantage of the

CU schemes over the staggered central schemes is that the CU schemes admit a particularly simple semi-discrete formulation. The 2-D extension of the semi-discrete CU schemes in [15, 16] was carried out in a straightforward "dimension-by-dimension" manner. Second- and third-order 2-D semi-discrete CU schemes were rigorously derived in [10, 12, 13], and a genuinely 2-D fully discrete CU scheme was introduced in [14].

In this paper, we develop a new way to perform the projection step, which leads to new semi-discrete low-dissipation CU (LDCU) schemes containing substantially reduced amount of numerical dissipation, especially in the contact wave areas and shear zones. A major novelty of our approach is that instead of using a sharper piecewise linear reconstruction of the intermediate solution (as in [10]), we now use a subcell resolution. In the 1-D case, we reconstruct the intermediate solution at each cell interface using two constant pieces for each component of $\boldsymbol{U}$. This way we will need to have $2d$ pieces of information at each cell interface, for which we will have d conservation requirements and d degrees of freedom, which can be used to ensure high accuracy of the projection step in the vicinities of contact waves. The 2-D extension of the new LDCU scheme is performed in a "dimension-by-dimension" approach, but taking into account specific properties of the quasi 1-D contact waves.

The new projection technique relies on the properties of contact waves of a particular hyperbolic system at hand. In this paper, we first consider the 1-D Euler equations of gas dynamics and enforce continuity of the velocity and pressure across the reconstructed intermediate solution at each cell interface. We then extend the 1-D LDCU numerical flux to the 2-D case. The extension is not straightforward as in 2-D, one has an additional degree of freedom related to the tangentional velocity.

The rest of the paper is organized as follows. In Sect. 2, we give an overview of the CU schemes. In Sect. 3.1, we develop the new projection step for the 1-D Euler equations of gas dynamics and use it to develop a new semi-discrete LDCU scheme. In Sect. 3.2, we present the 2-D extension of the new semi-discrete LDCU scheme. Finally, in Sect. 4, we test the proposed LDCU schemes on a number of 1-D and 2-D numerical examples and demonstrate the superiority of the proposed schemes over the CU schemes from [10].

2 Second-Order CU Schemes: An Overview

In this section, we provide an overview of the fully and semi-discrete second-order CU schemes for general 1-D hyperbolic systems of conservation laws (1.1).

We cover the computational domain with the finite volume cells $C_j = [x_{j-\frac{1}{2}}, x_{j+\frac{1}{2}}]$ centered at $x_j = (x_{j-\frac{1}{2}} + x_{j+\frac{1}{2}})/2$. For simplicity of presentation, we assume that the cells are uniform, that is, $x_{j+\frac{1}{2}} - x_{j-\frac{1}{2}} \equiv \Delta x$.

2.1 Fully Discrete CU Scheme

We assume that the solution, realized in terms of its cell averages $\overline{\boldsymbol{U}}_j^n := \frac{1}{\Delta x}\int_{C_j} \boldsymbol{U}(x,t^n)\,\mathrm{d}x$, is available at a certain time level $t = t^n$. In order to develop CU schemes, we follow the following three consecutive steps: *reconstruction*, *evolution*, and *projection*.

Reconstruction We reconstruct a second-order piecewise linear interpolant

$$\widetilde{\boldsymbol{U}}(x,t^n) = \sum_j \Big[\ \overline{\boldsymbol{U}}_j^n + (\boldsymbol{U}_x)_j^n (x - x_j)\Big]\chi_j(x), \tag{2.1}$$

where $\mathcal{X}_j(x)$ is the characteristic function of the cell C_j, $(\boldsymbol{U}_x)_j^n$ are the slopes which are supposed to be computed using a nonlinear limiter to ensure a non-oscillatory nature of (2.1). In the numerical experiments reported in Sect. 4, we have used a generalized minmod limiter (see, e.g., [21, 24, 32, 34]),

$$(\boldsymbol{U}_x)_j^n = \text{minmod}\left(\theta\,\frac{\overline{\boldsymbol{U}}_{j+1}^{\,n}-\overline{\boldsymbol{U}}_{j}^{\,n}}{\Delta x},\ \frac{\overline{\boldsymbol{U}}_{j+1}^{\,n}-\overline{\boldsymbol{U}}_{j-1}^{\,n}}{2\Delta x},\ \theta\,\frac{\overline{\boldsymbol{U}}_{j}^{\,n}-\overline{\boldsymbol{U}}_{j-1}^{\,n}}{\Delta x}\right),\quad \theta\in[1,2], \tag{2.2}$$

applied in a componentwise manner. Here, the minmod function is defined by

$$\text{minmod}(c_1,c_2,\ldots)=\begin{cases}\min(c_1,c_2,\ldots) & \text{if } c_i>0,\ \forall i,\\ \max(c_1,c_2,\ldots) & \text{if } c_i<0,\ \forall i,\\ 0 & \text{otherwise,}\end{cases} \tag{2.3}$$

and θ is used to control the oscillations: larger values of θ correspond to sharper but, in general, more oscillatory reconstructions.

Evolution CU schemes are Godunov-type schemes and thus the solution is evolved by integrating the system (1.1) over the space-time CVs. To this end, we recall that the reconstruction (2.1) is generically discontinuous at the cell interfaces $x=x_{j+\frac12}$ and the nonlinear waves generated there may also be discontinuous. On the other hand, they propagate with a finite speed, which makes it possible to contain all of the nonsmooth parts of the solution inside the CVs. In order to achieve this goal, we first need to evaluate the local speeds of propagation using the eigenvalues $\lambda_1(\boldsymbol{U})<\cdots<\lambda_d(\boldsymbol{U})$ of the Jacobian $\frac{\partial \boldsymbol{F}}{\partial \boldsymbol{U}}$. For instance, the left- and right-sided speeds can be estimated by

$$a^-_{j+\frac12}=\min\left\{\lambda_1\big(\boldsymbol{U}^-_{j+\frac12}\big),\lambda_1\big(\boldsymbol{U}^+_{j+\frac12}\big),0\right\},\quad a^+_{j+\frac12}=\max\left\{\lambda_d\big(\boldsymbol{U}^-_{j+\frac12}\big),\lambda_d\big(\boldsymbol{U}^+_{j+\frac12}\big),0\right\}, \tag{2.4}$$

where $\boldsymbol{U}^-_{j+\frac12}$ and $\boldsymbol{U}^+_{j+\frac12}$ denote the left- and right-sided values of the piecewise linear reconstruction (2.1)–(2.3) at $x=x_{j+\frac12}$, respectively:

$$\begin{aligned}\boldsymbol{U}^-_{j+\frac12}&=\lim_{x\to x^-_{j+\frac12}}\widetilde{\boldsymbol{U}}(x,t^n)=\overline{\boldsymbol{U}}_{j}^{\,n}+\frac{\Delta x}{2}(\boldsymbol{U}_x)_j^n,\\ \boldsymbol{U}^+_{j+\frac12}&=\lim_{x\to x^+_{j+\frac12}}\widetilde{\boldsymbol{U}}(x,t^n)=\overline{\boldsymbol{U}}_{j+1}^{\,n}-\frac{\Delta x}{2}(\boldsymbol{U}_x)_{j+1}^n.\end{aligned} \tag{2.5}$$

We then conclude that on the time interval $[t^n,t^{n+1}]$, where $t^{n+1}:=t^n+\Delta t^n$, the solution may be nonsmooth only inside the "nonsmooth" CVs $[x_{j+\frac12,\ell},x_{j+\frac12,r}]\times[t^n,t^{n+1}]$, where $x_{j+\frac12,\ell}:=x_{j+\frac12}+a^-_{j+\frac12}\Delta t^n$ and $x_{j+\frac12,r}:=x_{j+\frac12}+a^+_{j+\frac12}\Delta t^n$. In order to prevent the overlapping of the "nonsmooth" CVs, we use the CFL number 1/2 and set

$$\Delta t^n\le\frac{\Delta x}{2a_{\max}},\quad a_{\max}=\max_j\left\{\max\left(-a^-_{j+\frac12},a^+_{j+\frac12}\right)\right\}.$$

This condition ensures that $x_{j-\frac12,r}\le x_{j+\frac12,\ell}$ for all j. Moreover, since we use the one-sided local speeds of propagation to set up "nonsmooth" CVs, there will be gaps between the

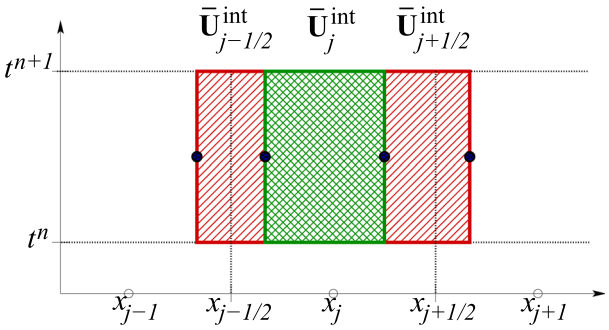

Fig. 1 "Nonsmooth" and "smooth" CVs

"nonsmooth" CVs, which we will fill in with the "smooth" ones, $[x_{j-\frac{1}{2},r}, x_{j+\frac{1}{2},\ell}]\times[t^n, t^{n+1}]$; see Fig. 1. This way, the entire computational domain will be covered with the CVs and we evolve the solution in each of them as follows.

First, we integrate the system (1.1) over the "nonsmooth" CVs to obtain

$$\begin{aligned}\overline{\boldsymbol{U}}^{\ \text{int}}_{j+\frac{1}{2}} &\approx \frac{1}{x_{j+\frac{1}{2},r}-x_{j+\frac{1}{2},\ell}}\int\limits_{x_{j+\frac{1}{2},\ell}}^{x_{j+\frac{1}{2},r}}\boldsymbol{U}(x,t^{n+1})\,\mathrm{d}x\\ &= \frac{1}{x_{j+\frac{1}{2},r}-x_{j+\frac{1}{2},\ell}}\Bigg[\int\limits_{x_{j+\frac{1}{2},\ell}}^{x_{j+\frac{1}{2},r}}\boldsymbol{U}(x,t^n)\,\mathrm{d}x-\int\limits_{t^n}^{t^{n+1}}\Big\{\boldsymbol{F}\big(\boldsymbol{U}(x_{j+\frac{1}{2},r},t)\big)\\ &\quad-\boldsymbol{F}\big(\boldsymbol{U}(x_{j+\frac{1}{2},\ell},t)\big)\Big\}\,\mathrm{d}t\Bigg].\end{aligned}\tag{2.6}$$

The spatial integral on the right-hand side (RHS) of (2.6) is evaluated exactly, while the temporal integral there is approximated using the midpoint rule. This results in

$$\begin{aligned}\overline{\boldsymbol{U}}^{\ \text{int}}_{j+\frac{1}{2}} &= \frac{1}{a^+_{j+\frac{1}{2}}-a^-_{j+\frac{1}{2}}}\Bigg\{\boldsymbol{U}^n_{j+\frac{1}{2},r}a^+_{j+\frac{1}{2}}-\frac{(\boldsymbol{U}_x)^n_{j+1}}{2}\big(a^+_{j+\frac{1}{2}}\big)^2\Delta t^n-\boldsymbol{U}^n_{j+\frac{1}{2},\ell}a^-_{j+\frac{1}{2}}\\ &\quad+\frac{(\boldsymbol{U}_x)^n_j}{2}\big(a^-_{j+\frac{1}{2}}\big)^2\Delta t^n-\Big[\boldsymbol{F}\big(\boldsymbol{U}^{n+\frac{1}{2}}_{j+\frac{1}{2},r}\big)-\boldsymbol{F}\big(\boldsymbol{U}^{n+\frac{1}{2}}_{j+\frac{1}{2},\ell}\big)\Big]\Bigg\},\end{aligned}\tag{2.7}$$

where

$$\begin{aligned}\boldsymbol{U}^{\,n}_{j+\frac{1}{2},\ell} &:= \widetilde{\boldsymbol{U}}(x_{j+\frac{1}{2},\ell},t^n) = \ \overline{\boldsymbol{U}}^{\ n}_{j}+(\boldsymbol{U}_x)^n_j\left(\frac{\Delta x}{2}+a^-_{j+\frac{1}{2}}\Delta t^n\right),\\ \boldsymbol{U}^{\,n}_{j+\frac{1}{2},r} &:= \widetilde{\boldsymbol{U}}(x_{j+\frac{1}{2},r},t^n) = \ \overline{\boldsymbol{U}}^{\ n}_{j+1}-(\boldsymbol{U}_x)^n_{j+1}\left(\frac{\Delta x}{2}-a^+_{j+\frac{1}{2}}\Delta t^n\right),\end{aligned}$$

are computed using the piecewise linear reconstruction (2.1), and the midpoint values, $\boldsymbol{U}^{n+\frac{1}{2}}_{j+\frac{1}{2},r}\approx\boldsymbol{U}\big(x_{j+\frac{1}{2},r},t^{n+\frac{1}{2}}\big)$ and $\boldsymbol{U}^{n+\frac{1}{2}}_{j+\frac{1}{2},\ell}\approx\boldsymbol{U}\big(x_{j+\frac{1}{2},\ell},t^{n+\frac{1}{2}}\big)$, are obtained using the Taylor expansions about $(x_{j+\frac{1}{2},r},t^n)$ and $(x_{j+\frac{1}{2},\ell},t^n)$, respectively, which gives

$$\boldsymbol{U}^{n+\frac{1}{2}}_{j+\frac{1}{2},\ell}=\boldsymbol{U}^n_{j+\frac{1}{2},\ell}-\frac{\Delta t^n}{2}\boldsymbol{F}\big(\boldsymbol{U}^n_{j+\frac{1}{2},\ell}\big)_x,\quad \boldsymbol{U}^{n+\frac{1}{2}}_{j+\frac{1}{2},r}=\boldsymbol{U}^n_{j+\frac{1}{2},r}-\frac{\Delta t^n}{2}\boldsymbol{F}\big(\boldsymbol{U}^n_{j+\frac{1}{2},r}\big)_x.\tag{2.8}$$

Here, the slopes $\boldsymbol{F}\big(\boldsymbol{U}^n_{j+\frac{1}{2},\ell}\big)_x$ and $\boldsymbol{F}\big(\boldsymbol{U}^n_{j+\frac{1}{2},r}\big)_x$ can be computed, for example, using the generalized minmod limiter; see [10] for details.

We then integrate the system (1.1) over the "smooth" CVs to obtain

$$\begin{aligned}\overline{\boldsymbol{U}}^{\,\text{int}}_{j} &\approx \frac{1}{x_{j+\frac{1}{2},\ell}-x_{j-\frac{1}{2},r}}\int\limits_{x_{j-\frac{1}{2},r}}^{x_{j+\frac{1}{2},\ell}}\boldsymbol{U}(x,t^{n+1})\,\mathrm{d}x\\ &= \frac{1}{x_{j+\frac{1}{2},\ell}-x_{j-\frac{1}{2},r}}\Bigg[\int\limits_{x_{j-\frac{1}{2},r}}^{x_{j+\frac{1}{2},\ell}}\boldsymbol{U}(x,t^n)\,\mathrm{d}x-\int\limits_{t^n}^{t^{n+1}}\Big\{\boldsymbol{F}\big(\boldsymbol{U}(x_{j+\frac{1}{2},\ell},t)\big)\\ &\quad-\boldsymbol{F}\big(\boldsymbol{U}(x_{j-\frac{1}{2},r},t)\big)\Big\}\,\mathrm{d}t\Bigg].\end{aligned}\tag{2.9}$$

The integrals on the RHS of (2.9) are evaluated precisely the same way of the integral on the RHS of (2.6), and this results in

$$\begin{aligned}\overline{\boldsymbol{U}}^{\,\text{int}}_{j} &= \overline{\boldsymbol{U}}^{\,n}_{j}+\frac{(\boldsymbol{U}_x)^n_j}{2}(a^+_{j-\frac{1}{2}}+a^-_{j+\frac{1}{2}})\Delta t^n\\ &\quad-\frac{\Delta t^n}{\Delta x-(a^+_{j-\frac{1}{2}}-a^-_{j+\frac{1}{2}})\Delta t^n}\Big[\boldsymbol{F}\big(\boldsymbol{U}^{n+\frac{1}{2}}_{j+\frac{1}{2},\ell}\big)-\boldsymbol{F}\big(\boldsymbol{U}^{n+\frac{1}{2}}_{j-\frac{1}{2},r}\big)\Big].\end{aligned}\tag{2.10}$$

Projection At the final step, we project the evolved solution, which is realized in terms of the intermediate cell averages $\{\overline{\boldsymbol{U}}^{\,\text{int}}_{j},\ \overline{\boldsymbol{U}}^{\,\text{int}}_{j+\frac{1}{2}}\}$ onto the original grid. In order to ensure the second order of the resulting scheme, we first need to reconstruct a piecewise linear interpolant

$$\widetilde{\boldsymbol{U}}^{\,\text{int}}(x)=\sum_j\Big\{\widetilde{\boldsymbol{U}}^{\,\text{int}}_{j+\frac{1}{2}}(x)\mathcal{X}_{[x_{j+\frac{1}{2},\ell},x_{j+\frac{1}{2},r}]}+\overline{\boldsymbol{U}}^{\,\text{int}}_{j}\mathcal{X}_{[x_{j-\frac{1}{2},r},x_{j+\frac{1}{2},\ell}]}\Big\},\tag{2.11}$$

sketched in Fig. 2. Here,

$$\widetilde{\boldsymbol{U}}^{\,\text{int}}_{j+\frac{1}{2}}(x)=\overline{\boldsymbol{U}}^{\,\text{int}}_{j+\frac{1}{2}}+(\boldsymbol{U}_x)^{\text{int}}_{j+\frac{1}{2}}\left(x-\frac{x_{j+\frac{1}{2},r}+x_{j+\frac{1}{2},\ell}}{2}\right),\tag{2.12}$$

where the slopes $(\boldsymbol{U}_x)^{\text{int}}_{j+\frac{1}{2}}$ in (2.11) can be computed, for instance, as in [10]:

$$\begin{aligned}(\boldsymbol{U}_x)^{\text{int}}_{j+\frac{1}{2}}&=\text{minmod}\left(\frac{\boldsymbol{U}^{\text{int}}_{j+\frac{1}{2},r}-\overline{\boldsymbol{U}}^{\,\text{int}}_{j+\frac{1}{2}}}{\delta},\frac{\overline{\boldsymbol{U}}^{\,\text{int}}_{j+\frac{1}{2}}-\boldsymbol{U}^{\text{int}}_{j+\frac{1}{2},\ell}}{\delta}\right),\\ \delta&:=\frac{\Delta t^n}{2}\big(a^+_{j+\frac{1}{2}}-a^-_{j+\frac{1}{2}}\big),\end{aligned}\tag{2.13}$$

and similarly to (2.8), $\boldsymbol{U}^{\text{int}}_{j+\frac{1}{2},\ell}\approx\boldsymbol{U}(x_{j+\frac{1}{2},\ell},t^{n+1})$ and $\boldsymbol{U}^{\text{int}}_{j+\frac{1}{2},r}\approx\boldsymbol{U}(x_{j+\frac{1}{2},r},t^{n+1})$ are evaluated using the Taylor expansions:

$$\boldsymbol{U}^{\text{int}}_{j+\frac{1}{2},r}=\boldsymbol{U}^n_{j+\frac{1}{2},r}-\Delta t^n\boldsymbol{F}\big(\boldsymbol{U}^n_{j+\frac{1}{2},r}\big)_x,\quad\boldsymbol{U}^{\text{int}}_{j+\frac{1}{2},\ell}=\boldsymbol{U}^n_{j+\frac{1}{2},\ell}-\Delta t^n\boldsymbol{F}\big(\boldsymbol{U}^n_{j+\frac{1}{2},\ell}\big)_x.\tag{2.14}$$

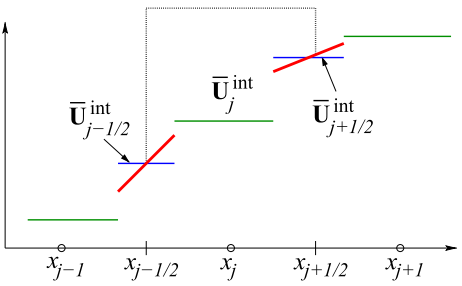

Fig. 2 Piecewise linear interpolant (2.11) and its projection onto the cell C_j

Equipped with the piecewise linear interpolant $\widetilde{\boldsymbol{U}}^{\,\mathrm{int}}$, we average it over the cell C_j to end up with

$$\begin{aligned}\overline{\boldsymbol{U}}^{\,n+1}_{j} = \frac{1}{\Delta x}\int\limits_{C_j}\widetilde{\boldsymbol{U}}^{\,\mathrm{int}}(x)\,\mathrm{d}x = \overline{\boldsymbol{U}}^{\,\mathrm{int}}_{j} + \frac{\Delta t^n}{\Delta x}\Big[a^+_{j-\frac12}\big(\overline{\boldsymbol{U}}^{\,\mathrm{int}}_{j-\frac12} - \overline{\boldsymbol{U}}^{\,\mathrm{int}}_{j}\big)\\ - a^-_{j+\frac12}\big(\overline{\boldsymbol{U}}^{\,\mathrm{int}}_{j+\frac12} - \overline{\boldsymbol{U}}^{\,\mathrm{int}}_{j}\big)\\ + \frac{\Delta t^n}{2}\big\{a^+_{j+\frac12}a^-_{j+\frac12}(\boldsymbol{U}_x)^{n+1}_{j+\frac12} - a^+_{j-\frac12}a^-_{j-\frac12}(\boldsymbol{U}_x)^{n+1}_{j-\frac12}\big\}\Big].\end{aligned} \tag{2.15}$$

This completes the construction of the fully discrete second-order CU scheme, which is quite complicated, but admits a very simple semi-discrete form.

Remark 2.1 We note that the slopes $(\boldsymbol{U}_x)^{\,\mathrm{int}}_{j+\frac12}$ in (2.12) have to be at least first-order approximations of the spatial derivatives at the centers of the intervals $[x_{j+\frac12,\ell}, x_{j+\frac12,r}]$. This is required in order to keep the resulting fully discrete CU scheme to be second order.

2.2 Semi-Discrete CU Scheme

We now reduce the fully discrete scheme from Sect. 2.1 to the semi-discrete form by taking the following temporal limit:

$$\begin{aligned}\frac{\mathrm{d}}{\mathrm{dt}}\,\overline{\boldsymbol{U}}_j(t^n) = \lim_{\Delta t^n\to 0}\frac{\overline{\boldsymbol{U}}^{\,n+1}_{j} - \overline{\boldsymbol{U}}^{\,n}_{j}}{\Delta t^n} = \lim_{\Delta t^n\to 0}\frac{\overline{\boldsymbol{U}}^{\,\mathrm{int}}_{j} - \overline{\boldsymbol{U}}^{\,n}_{j}}{\Delta t^n}\\ + \frac{1}{\Delta x}\Big[a^+_{j-\frac12}\lim_{\Delta t^n\to 0}\overline{\boldsymbol{U}}^{\,\mathrm{int}}_{j-\frac12} + \big(a^-_{j+\frac12} - a^+_{j-\frac12}\big)\lim_{\Delta t^n\to 0}\overline{\boldsymbol{U}}^{\,\mathrm{int}}_{j} - a^-_{j+\frac12}\lim_{\Delta t^n\to 0}\overline{\boldsymbol{U}}^{\,\mathrm{int}}_{j+\frac12}\\ + \frac12 a^+_{j+\frac12}a^-_{j+\frac12}\lim_{\Delta t^n\to 0}\big\{\Delta t^n(\boldsymbol{U}_x)^{\,\mathrm{int}}_{j+\frac12}\big\} - \frac12 a^+_{j-\frac12}a^-_{j-\frac12}\lim_{\Delta t^n\to 0}\big\{\Delta t^n(\boldsymbol{U}_x)^{\,\mathrm{int}}_{j-\frac12}\big\}\Big].\end{aligned} \tag{2.16}$$

This limit is evaluated by substituting (2.7) and (2.10) into (2.16), which results in the second-order semi-discrete CU scheme:

$$\frac{\mathrm{d}}{\mathrm{dt}}\,\overline{\boldsymbol{U}}_j(t) = -\frac{\boldsymbol{\mathcal{F}}_{j+\frac12}(t) - \boldsymbol{\mathcal{F}}_{j-\frac12}(t)}{\Delta x}, \tag{2.17}$$

where $\boldsymbol{\mathcal{F}}_{j+\frac12}$ are CU numerical fluxes given by

$$\boldsymbol{\mathcal{F}}_{j+\frac12} = \frac{a^+_{j+\frac12}\boldsymbol{F}\big(\boldsymbol{U}^-_{j+\frac12}\big) - a^-_{j+\frac12}\boldsymbol{F}\big(\boldsymbol{U}^+_{j+\frac12}\big)}{a^+_{j+\frac12} - a^-_{j+\frac12}}$$

$$+\frac{a^+_{j+\frac12}a^-_{j+\frac12}}{a^+_{j+\frac12}-a^-_{j+\frac12}}\left[\boldsymbol{U}^+_{j+\frac12}-\boldsymbol{U}^-_{j+\frac12}-\delta\boldsymbol{U}_{j+\frac12}\right]. \tag{2.18}$$

Here, $\delta\boldsymbol{U}_{j+\frac12}$ is the "built-in" anti-diffusion term given by

$$\begin{aligned}\delta\boldsymbol{U}_{j+\frac12}&=\frac{a^+_{j+\frac12}-a^-_{j+\frac12}}{2}\lim_{\Delta t^n\to0}\left\{\Delta t^n(\boldsymbol{U}_x)^{\text{int}}_{j+\frac12}\right\}\\&=\text{minmod}\left(\boldsymbol{U}^+_{j+\frac12}-\boldsymbol{U}^*_{j+\frac12},\boldsymbol{U}^*_{j+\frac12}-\boldsymbol{U}^-_{j+\frac12}\right)\end{aligned} \tag{2.19}$$

with $\boldsymbol{U}^*_{j+\frac12}$ obtained by passing to the limit in (2.7), namely,

$$\boldsymbol{U}^*_{j+\frac12}=\lim_{\Delta t^n\to0}\overline{\boldsymbol{U}}^{\text{int}}_{j+\frac12}=\frac{a^+_{j+\frac12}\boldsymbol{U}^+_{j+\frac12}-a^-_{j+\frac12}\boldsymbol{U}^-_{j+\frac12}-\left\{\boldsymbol{F}\left(\boldsymbol{U}^+_{j+\frac12}\right)-\boldsymbol{F}\left(\boldsymbol{U}^-_{j+\frac12}\right)\right\}}{a^+_{j+\frac12}-a^-_{j+\frac12}}. \tag{2.20}$$

Note that all of the indexed quantities in (2.18)–(2.20) are time dependent, but from now on we will omit this dependence for the sake of brevity.

Remark 2.2 We note that when the 1-D schemes are implemented, the computation of the CU numerical fluxes in (2.18) needs to be desingularized at those cell interfaces $x=x_{j+\frac12}$ where both of the local speeds are very small. This means that wherever $a^+_{j+\frac12}-a^-_{j+\frac12}<\varepsilon$ for a small positive ε, we replace (2.18) with

$$\boldsymbol{\mathcal{F}}_{j+\frac12}=\frac{\boldsymbol{F}(\boldsymbol{U}^-_{j+\frac12})+\boldsymbol{F}(\boldsymbol{U}^+_{j+\frac12})}{2}.$$

Remark 2.3 The semi-discretization (2.17) is a system of time-dependent ODEs, which has to be numerically integrated. In all of the numerical experiments reported in Sect. 4.1, we have used the three-stage third-order strong stability preserving (SSP) Runge-Kutta method; see, e.g., [7, 8].

Remark 2.4 We stress that the order of accuracy of the semi-discretization (2.17)–(2.20) is determined by the order of reconstruction of $\boldsymbol{U}^{\pm}_{j+\frac12}$ and is independent on the accuracy of the projection step as the size of the interval $[x_{j+\frac12,\ell},x_{j+\frac12,r}]$ shrinks to 0 when $\Delta t^n\to0$. Thus, even if we take $(\boldsymbol{U}_x)^{\text{int}}_{j+\frac12}\equiv0$, which would remove the anti-diffusion term $\delta\boldsymbol{U}_{j+\frac12}$ from the CU numerical flux (2.18) and reduce the scheme (2.17)–(2.20) to the original CU scheme from [12], the formal order of accuracy will still be determined by the accuracy $\boldsymbol{U}^{\pm}_{j+\frac12}$ are computed with.

3 A New Family of the LDCU Schemes

In this section, we present a new family of the LDCU schemes. Our goal is to further reduce the amount of numerical dissipation present in the CU schemes without risking oscillations.

First, we recall that the amount of dissipation present in both fully and semi-discrete CU schemes can be controlled by the way the projection step is conducted. This, in fact, boils down

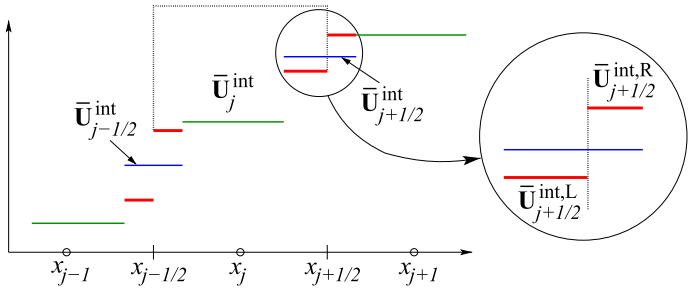

Fig. 3 The new projection step

to the way the slopes $(\boldsymbol{U}_x)^{\text{int}}_{j+\frac{1}{2}}$ are evaluated. Formulae (2.13)–(2.14) lead to an intermediate reconstruction (2.11), which is much sharper than the one used in the original papers [12, 15], and thus to the "built-in" anti-diffusion term (2.19)–(2.20) appearing in the CU numerical flux (2.18). However, the use of the linear pieces (2.12), which is necessary to ensure the second order of accuracy of fully discrete CU schemes, has its limitations as these pieces are continuous across the cell interfaces $x = x_{j+\frac{1}{2}}$. As mentioned in Remark 2.3, preserving high order of the semi-discrete CU scheme is easier and this gives us more flexibility in designing the projection step.

We therefore propose a new and completely different projection procedure. Instead of the linear piece (2.12), we will use a subcell resolution approach and replace (2.12) with

$$\widetilde{\boldsymbol{U}}^{\text{int}}_{j+\frac{1}{2}}(x) = \begin{cases} \overline{\boldsymbol{U}}^{\text{int,L}}_{j+\frac{1}{2}}, & x < x_{j+\frac{1}{2}}, \\ \overline{\boldsymbol{U}}^{\text{int,R}}_{j+\frac{1}{2}}, & x > x_{j+\frac{1}{2}}, \end{cases} \tag{3.1}$$

which consists of two constant pieces; see Fig. 3. Notice that (3.1) is generically discontinuous at $x = x_{j+\frac{1}{2}}$ and one can take an advantage of this fact in order to design a very sharp intermediate interpolation (2.11), (3.1). We also note that (3.1) contains $2d$ pieces of information. The conservation property of (3.1) will be enforced by requiring the following d relations between $\overline{\boldsymbol{U}}^{\text{int,L}}_{j+\frac{1}{2}}$ and $\overline{\boldsymbol{U}}^{\text{int,R}}_{j+\frac{1}{2}}$ quantities to be satisfied:

$$a^{+}_{j+\frac{1}{2}}\,\overline{\boldsymbol{U}}^{\text{int,R}}_{j+\frac{1}{2}} - a^{-}_{j+\frac{1}{2}}\,\overline{\boldsymbol{U}}^{\text{int,L}}_{j+\frac{1}{2}} = (a^{+}_{j+\frac{1}{2}} - a^{-}_{j+\frac{1}{2}})\,\overline{\boldsymbol{U}}^{\text{int}}_{j+\frac{1}{2}}. \tag{3.2}$$

This leaves one with d degrees of freedom, which can be used to improve the quality of the local approximation achieved by (3.1). We propose to use these degrees of freedom in order to improve the resolution of linearly degenerate contact waves, which are typically much harder to accurately capture due to their linear nature and lack of the self-sharpening mechanisms possessed by the nonlinear shock waves. In order to achieve this goal, we will use specific properties of the contact waves arising in the studied hyperbolic systems of conservation laws. In the rest of the paper, we restrict our consideration to the Euler equation of gas dynamics.

3.1 New LDCU Scheme for the 1-D Euler Equations of Gas Dynamics

The 1-D Euler equations of gas dynamics reads as (1.1) with

$$\boldsymbol{U}=\begin{pmatrix}\rho\\ \rho u\\ E\end{pmatrix}\quad\text{and}\quad \boldsymbol{F}(\boldsymbol{U})=\begin{pmatrix}\rho u\\ \rho u^2+p\\ u(E+p)\end{pmatrix}, \tag{3.3}$$

where ρ is the density, u is the velocity, p is the pressure, and E is the total energy. The system (1.1), (3.3) is closed using the equation of states (EOS), which is in the case of ideal gas is

$$p=(\gamma-1)\Big[E-\frac{1}{2}\rho u^2\Big],\quad \gamma=\text{Const}. \tag{3.4}$$

In order to develop the new CU scheme for the system (1.1), (3.3), (3.4), we first use the generalized minmod reconstruction (2.2), (2.3), (2.5) to obtain the point values $\rho^{\pm}_{j+\frac{1}{2}}$, $(\rho u)^{\pm}_{j+\frac{1}{2}}$ and $E^{\pm}_{j+\frac{1}{2}}$, which can be used to evaluate the corresponding point values of u and p:

$$u^{\pm}_{j+\frac{1}{2}}=\frac{(\rho u)^{\pm}_{j+\frac{1}{2}}}{\rho^{\pm}_{j+\frac{1}{2}}},\quad p^{\pm}_{j+\frac{1}{2}}=(\gamma-1)\Big[E^{\pm}_{j+\frac{1}{2}}-\frac{1}{2}\rho^{\pm}_{j+\frac{1}{2}}\big(u^{\pm}_{j+\frac{1}{2}}\big)^2\Big]. \tag{3.5}$$

We then estimate the one-sided local speeds of propagation according to (2.4), which reduces to

$$\begin{aligned}a^{-}_{j+\frac{1}{2}}&=\min\Big\{u^{+}_{j+\frac{1}{2}}-c^{+}_{j+\frac{1}{2}},u^{-}_{j+\frac{1}{2}}-c^{-}_{j+\frac{1}{2}},0\Big\},\\ a^{+}_{j+\frac{1}{2}}&=\max\Big\{u^{+}_{j+\frac{1}{2}}+c^{+}_{j+\frac{1}{2}},u^{-}_{j+\frac{1}{2}}+c^{-}_{j+\frac{1}{2}},0\Big\},\end{aligned}$$

where $c^{\pm}_{j+\frac{1}{2}}=\sqrt{\gamma p^{\pm}_{j+\frac{1}{2}}/\rho^{\pm}_{j+\frac{1}{2}}}$ are the corresponding point values of the speed of sound.

We then proceed with the evolution of the subcell averages $\overline{\boldsymbol{U}}^{\,\text{int,L}}_{j+\frac{1}{2}}=\big(\overline{\rho}^{\,\text{int,L}}_{j+\frac{1}{2}},(\overline{\rho u})^{\text{int,L}}_{j+\frac{1}{2}},\overline{E}^{\,\text{int,L}}_{j+\frac{1}{2}}\big)^{\top}$ and $\overline{\boldsymbol{U}}^{\,\text{int,R}}_{j+\frac{1}{2}}=\big(\overline{\rho}^{\,\text{int,R}}_{j+\frac{1}{2}},(\overline{\rho u})^{\text{int,R}}_{j+\frac{1}{2}},\overline{E}^{\,\text{int,R}}_{j+\frac{1}{2}}\big)^{\top}$ required in (3.1). Our goal is to develop a new projection procedure designed to accurately approximate isolated contact waves, which consist of jump discontinuities in ρ propagating in the region with constant u and p. We therefore use two of the remaining three degrees of freedom to enforce the continuity of u and p across the cell interfaces by setting

$$\frac{(\overline{\rho u})^{\text{int,L}}_{j+\frac{1}{2}}}{\overline{\rho}^{\,\text{int,L}}_{j+\frac{1}{2}}}=\frac{(\overline{\rho u})^{\text{int,R}}_{j+\frac{1}{2}}}{\overline{\rho}^{\,\text{int,R}}_{j+\frac{1}{2}}},\quad \overline{E}^{\,\text{int,L}}_{j+\frac{1}{2}}-\frac{\big((\overline{\rho u})^{\text{int,L}}_{j+\frac{1}{2}}\big)^2}{2\,\overline{\rho}^{\,\text{int,L}}_{j+\frac{1}{2}}}=\overline{E}^{\,\text{int,R}}_{j+\frac{1}{2}}-\frac{\big((\overline{\rho u})^{\text{int,R}}_{j+\frac{1}{2}}\big)^2}{2\,\overline{\rho}^{\,\text{int,R}}_{j+\frac{1}{2}}}, \tag{3.6}$$

where we have used the EOS (3.4). Next, (3.6) together with the conservation requirement for ρu and E, namely (see (3.2)),

$$\begin{aligned}a^{+}_{j+\frac{1}{2}}(\overline{\rho u})^{\text{int,R}}_{j+\frac{1}{2}}-a^{-}_{j+\frac{1}{2}}(\overline{\rho u})^{\text{int,L}}_{j+\frac{1}{2}}&=\big(a^{+}_{j+\frac{1}{2}}-a^{-}_{j+\frac{1}{2}}\big)(\overline{\rho u})^{\text{int}}_{j+\frac{1}{2}},\\ a^{+}_{j+\frac{1}{2}}\,\overline{E}^{\,\text{int,R}}_{j+\frac{1}{2}}-a^{-}_{j+\frac{1}{2}}\,\overline{E}^{\,\text{int,L}}_{j+\frac{1}{2}}&=\big(a^{+}_{j+\frac{1}{2}}-a^{-}_{j+\frac{1}{2}}\big)\,\overline{E}^{\,\text{int}}_{j+\frac{1}{2}},\end{aligned}$$

form a system of four algebraic equations equations, which we solve for $(\overline{\rho u})^{\mathrm{int,L}}_{j+\frac{1}{2}}$, $(\overline{\rho u})^{\mathrm{int,R}}_{j+\frac{1}{2}}$, $\overline{E}^{\mathrm{int,L}}_{j+\frac{1}{2}}$, and $\overline{E}^{\mathrm{int,R}}_{j+\frac{1}{2}}$, and express these quantities in terms of $\overline{\rho}^{\mathrm{int,L}}_{j+\frac{1}{2}}$ and $\overline{\rho}^{\mathrm{int,R}}_{j+\frac{1}{2}}$:

$$
\begin{aligned}
(\overline{\rho u})^{\mathrm{int,L}}_{j+\frac{1}{2}} &= \frac{\left(a^+_{j+\frac{1}{2}} - a^-_{j+\frac{1}{2}}\right)\overline{\rho}^{\mathrm{int,L}}_{j+\frac{1}{2}}}{a^+_{j+\frac{1}{2}}\overline{\rho}^{\mathrm{int,R}}_{j+\frac{1}{2}} - a^-_{j+\frac{1}{2}}\overline{\rho}^{\mathrm{int,L}}_{j+\frac{1}{2}}}(\overline{\rho u})^{\mathrm{int}}_{j+\frac{1}{2}},\\
(\overline{\rho u})^{\mathrm{int,R}}_{j+\frac{1}{2}} &= \frac{\left(a^+_{j+\frac{1}{2}} - a^-_{j+\frac{1}{2}}\right)\overline{\rho}^{\mathrm{int,R}}_{j+\frac{1}{2}}}{a^+_{j+\frac{1}{2}}\overline{\rho}^{\mathrm{int,R}}_{j+\frac{1}{2}} - a^-_{j+\frac{1}{2}}\overline{\rho}^{\mathrm{int,L}}_{j+\frac{1}{2}}}(\overline{\rho u})^{\mathrm{int}}_{j+\frac{1}{2}},\\
\overline{E}^{\mathrm{int,L}}_{j+\frac{1}{2}} &= \overline{E}^{\mathrm{int}}_{j+\frac{1}{2}} + \frac{a^+_{j+\frac{1}{2}}\left(a^+_{j+\frac{1}{2}} - a^-_{j+\frac{1}{2}}\right)\left(\overline{\rho}^{\mathrm{int,L}}_{j+\frac{1}{2}} - \overline{\rho}^{\mathrm{int,R}}_{j+\frac{1}{2}}\right)}{2\left(a^+_{j+\frac{1}{2}}\overline{\rho}^{\mathrm{int,R}}_{j+\frac{1}{2}} - a^-_{j+\frac{1}{2}}\overline{\rho}^{\mathrm{int,L}}_{j+\frac{1}{2}}\right)^2}\left((\overline{\rho u})^{\mathrm{int}}_{j+\frac{1}{2}}\right)^2,\\
\overline{E}^{\mathrm{int,R}}_{j+\frac{1}{2}} &= \overline{E}^{\mathrm{int}}_{j+\frac{1}{2}} + \frac{a^-_{j+\frac{1}{2}}\left(a^+_{j+\frac{1}{2}} - a^-_{j+\frac{1}{2}}\right)\left(\overline{\rho}^{\mathrm{int,L}}_{j+\frac{1}{2}} - \overline{\rho}^{\mathrm{int,R}}_{j+\frac{1}{2}}\right)}{2\left(a^+_{j+\frac{1}{2}}\overline{\rho}^{\mathrm{int,R}}_{j+\frac{1}{2}} - a^-_{j+\frac{1}{2}}\overline{\rho}^{\mathrm{int,L}}_{j+\frac{1}{2}}\right)^2}\left((\overline{\rho u})^{\mathrm{int}}_{j+\frac{1}{2}}\right)^2.
\end{aligned}
\tag{3.7}
$$

We finally need to determine $\overline{\rho}^{\mathrm{int,L}}_{j+\frac{1}{2}}$ and $\overline{\rho}^{\mathrm{int,R}}_{j+\frac{1}{2}}$, which are related by the conservation requirement for ρ, namely (see (3.2)),

$$
a^+_{j+\frac{1}{2}}\overline{\rho}^{\mathrm{int,R}}_{j+\frac{1}{2}} - a^-_{j+\frac{1}{2}}\overline{\rho}^{\mathrm{int,L}}_{j+\frac{1}{2}} = \left(a^+_{j+\frac{1}{2}} - a^-_{j+\frac{1}{2}}\right)\overline{\rho}^{\mathrm{int}}_{j+\frac{1}{2}},
\tag{3.8}
$$

leaving us with one remaining degree of freedom. Since we would like to have the sharpest (yet non-oscillatory) approximation of the jump in ρ, we need to make the difference $\overline{\rho}^{\mathrm{int,R}}_{j+\frac{1}{2}} - \overline{\rho}^{\mathrm{int,L}}_{j+\frac{1}{2}}$ as close as possible to $\rho^{\mathrm{int}}_{j+\frac{1}{2},r} - \rho^{\mathrm{int}}_{j+\frac{1}{2},\ell}$, but without creating any new local extrema in ρ, that is, ensuring that

$$
\min\left\{\rho^{\mathrm{int}}_{j+\frac{1}{2},\ell},\ \overline{\rho}^{\mathrm{int}}_{j+\frac{1}{2}},\ \rho^{\mathrm{int}}_{j+\frac{1}{2},r}\right\} \le \overline{\rho}^{\mathrm{int,L(R)}}_{j+\frac{1}{2}} \le \max\left\{\rho^{\mathrm{int}}_{j+\frac{1}{2},\ell},\ \overline{\rho}^{\mathrm{int}}_{j+\frac{1}{2}},\ \rho^{\mathrm{int}}_{j+\frac{1}{2},r}\right\},
\tag{3.9}
$$

where $\rho^{\mathrm{int}}_{j+\frac{1}{2},\ell}$ and $\rho^{\mathrm{int}}_{j+\frac{1}{2},r}$ are predicted using (2.14). In order to achieve this goal, we denote by

$$
S^-_{j+\frac{1}{2}} := -a^-_{j+\frac{1}{2}}\left(\overline{\rho}^{\mathrm{int}}_{j+\frac{1}{2}} - \rho^{\mathrm{int}}_{j+\frac{1}{2},\ell}\right) \quad \text{and} \quad S^+_{j+\frac{1}{2}} := a^+_{j+\frac{1}{2}}\left(\rho^{\mathrm{int}}_{j+\frac{1}{2},r} - \overline{\rho}^{\mathrm{int}}_{j+\frac{1}{2}}\right),
\tag{3.10}
$$

and then determine $\overline{\rho}^{\mathrm{int,L}}_{j+\frac{1}{2}}$ and $\overline{\rho}^{\mathrm{int,R}}_{j+\frac{1}{2}}$ according to the following algorithm.

Algorithm 3.1 (Computation of $\overline{\rho}^{\mathrm{int,L}}_{j+\frac{1}{2}}$ and $\overline{\rho}^{\mathrm{int,R}}_{j+\frac{1}{2}}$)

- *If* $S^-_{j+\frac{1}{2}} S^+_{j+\frac{1}{2}} \ge 0$, *then set*

$$
\overline{\rho}^{\mathrm{int,L}}_{j+\frac{1}{2}} = \overline{\rho}^{\mathrm{int}}_{j+\frac{1}{2}} \quad \text{and} \quad \overline{\rho}^{\mathrm{int,R}}_{j+\frac{1}{2}} = \overline{\rho}^{\mathrm{int}}_{j+\frac{1}{2}},
\tag{3.11}
$$

to avoid creation of new local extrema;

- *If* $S^-_{j+\frac{1}{2}} S^+_{j+\frac{1}{2}} < 0$ *and* $|S^-_{j+\frac{1}{2}}| < |S^+_{j+\frac{1}{2}}|$, *then set*

$$\overline{\rho}^{\,\mathrm{int,L}}_{j+\frac{1}{2}} = \rho^{\mathrm{int}}_{j+\frac{1}{2},\ell}, \qquad \overline{\rho}^{\,\mathrm{int,R}}_{j+\frac{1}{2}} = \frac{\left(a^+_{j+\frac{1}{2}} - a^-_{j+\frac{1}{2}}\right)\overline{\rho}^{\,\mathrm{int}}_{j+\frac{1}{2}} + a^-_{j+\frac{1}{2}}\,\overline{\rho}^{\,\mathrm{int,L}}_{j+\frac{1}{2}}}{a^+_{j+\frac{1}{2}}}; \tag{3.12}$$

- *If* $S^-_{j+\frac{1}{2}} S^+_{j+\frac{1}{2}} < 0$ *and* $|S^-_{j+\frac{1}{2}}| > |S^+_{j+\frac{1}{2}}|$, *then set*

$$\overline{\rho}^{\,\mathrm{int,R}}_{j+\frac{1}{2}} = \rho^{\mathrm{int}}_{j+\frac{1}{2},r}, \qquad \overline{\rho}^{\,\mathrm{int,L}}_{j+\frac{1}{2}} = \frac{\left(a^+_{j+\frac{1}{2}} - a^-_{j+\frac{1}{2}}\right)\overline{\rho}^{\,\mathrm{int}}_{j+\frac{1}{2}} - a^+_{j+\frac{1}{2}}\,\overline{\rho}^{\,\mathrm{int,R}}_{j+\frac{1}{2}}}{-a^-_{j+\frac{1}{2}}}. \tag{3.13}$$

Remark 3.1 It is easy to verify that the values $\overline{\rho}^{\,\mathrm{int,L}}_{j+\frac{1}{2}}$ and $\overline{\rho}^{\,\mathrm{int,R}}_{j+\frac{1}{2}}$ computed in either (3.11), (3.12), or (3.13) satisfy both the conservation (3.8) and non-oscillatory (3.9) requirements.

Remark 3.2 Notice that formulae (3.11)–(3.13) can be written in a compact form as

$$\begin{aligned} \overline{\rho}^{\,\mathrm{int,L}}_{j+\frac{1}{2}} &= \overline{\rho}^{\,\mathrm{int}}_{j+\frac{1}{2}} + \frac{\delta_{j+\frac{1}{2}}}{a^-_{j+\frac{1}{2}}}, \qquad \overline{\rho}^{\,\mathrm{int,R}}_{j+\frac{1}{2}} = \overline{\rho}^{\,\mathrm{int}}_{j+\frac{1}{2}} + \frac{\delta_{j+\frac{1}{2}}}{a^+_{j+\frac{1}{2}}}, \quad \delta_{j+\frac{1}{2}} \\ &:= \mathrm{minmod}(S^-_{j+\frac{1}{2}}, S^+_{j+\frac{1}{2}}), \end{aligned} \tag{3.14}$$

which, in turn, can be substituted into (3.7) to simplify it and obtain

$$\begin{gathered} (\overline{\rho u})^{\mathrm{int,L}}_{j+\frac{1}{2}} = (\overline{\rho u})^{\mathrm{int}}_{j+\frac{1}{2}} + \frac{\delta_{j+\frac{1}{2}}}{a^-_{j+\frac{1}{2}}} u^{\mathrm{int}}_{j+\frac{1}{2}}, \qquad (\overline{\rho u})^{\mathrm{int,R}}_{j+\frac{1}{2}} = (\overline{\rho u})^{\mathrm{int}}_{j+\frac{1}{2}} + \frac{\delta_{j+\frac{1}{2}}}{a^+_{j+\frac{1}{2}}} u^{\mathrm{int}}_{j+\frac{1}{2}}, \\ \overline{E}^{\,\mathrm{int,L}}_{j+\frac{1}{2}} = \overline{E}^{\,\mathrm{int}}_{j+\frac{1}{2}} + \frac{\delta_{j+\frac{1}{2}}}{2a^-_{j+\frac{1}{2}}} (u^{\mathrm{int}}_{j+\frac{1}{2}})^2, \qquad \overline{E}^{\,\mathrm{int,R}}_{j+\frac{1}{2}} = \overline{E}^{\,\mathrm{int}}_{j+\frac{1}{2}} + \frac{\delta_{j+\frac{1}{2}}}{2a^+_{j+\frac{1}{2}}} (u^{\mathrm{int}}_{j+\frac{1}{2}})^2, \\ u^{\mathrm{int}}_{j+\frac{1}{2}} := \frac{(\overline{\rho u})^{\mathrm{int}}_{j+\frac{1}{2}}}{\overline{\rho}^{\,\mathrm{int}}_{j+\frac{1}{2}}}. \end{gathered} \tag{3.15}$$

3.1.1 Fully Discrete Scheme

We now derive a new fully discrete LDCU scheme based on the new projection step. To this end, we integrate the piecewise constant interpolant (2.11), (3.1) over the cell C_j and obtain (compare with (2.15)) for ρ:

$$\begin{aligned} \overline{\rho}^{\,n+1}_{j} &= \overline{\rho}^{\,\mathrm{int}}_{j} + \frac{\Delta t^n}{\Delta x}\left[a^+_{j-\frac{1}{2}}\left(\overline{\rho}^{\,\mathrm{int,R}}_{j-\frac{1}{2}} - \overline{\rho}^{\,\mathrm{int}}_{j}\right) - a^-_{j+\frac{1}{2}}\left(\overline{\rho}^{\,\mathrm{int,L}}_{j+\frac{1}{2}} - \overline{\rho}^{\,\mathrm{int}}_{j}\right)\right] \\ &\overset{(3.14)}{=} \overline{\rho}^{\,\mathrm{int}}_{j} + \frac{\Delta t^n}{\Delta x}\left[a^+_{j-\frac{1}{2}}\left(\overline{\rho}^{\,\mathrm{int}}_{j-\frac{1}{2}} - \overline{\rho}^{\,\mathrm{int}}_{j}\right)\right. \\ &\quad \left. - a^-_{j+\frac{1}{2}}\left(\overline{\rho}^{\,\mathrm{int}}_{j+\frac{1}{2}} - \overline{\rho}^{\,\mathrm{int}}_{j}\right) + \delta_{j-\frac{1}{2}} - \delta_{j+\frac{1}{2}}\right], \end{aligned} \tag{3.16}$$

for ρu:

$$\begin{aligned}
(\,\overline{\rho u}\,)_j^{n+1} &= (\,\overline{\rho u}\,)_j^{\text{int}} + \frac{\Delta t^n}{\Delta x}\Big[a^+_{j-\frac{1}{2}}\big((\,\overline{\rho u}\,)^{\text{int,R}}_{j-\frac{1}{2}} - (\,\overline{\rho u}\,)_j^{\text{int}}\big) \\
&\quad - a^-_{j+\frac{1}{2}}\big((\,\overline{\rho u}\,)^{\text{int,L}}_{j+\frac{1}{2}} - (\,\overline{\rho u}\,)_j^{\text{int}}\big)\Big] \\
&\overset{(3.15)}{=} (\,\overline{\rho u}\,)_j^{\text{int}} + \frac{\Delta t^n}{\Delta x}\Big[a^+_{j-\frac{1}{2}}\big((\,\overline{\rho u}\,)^{\text{int}}_{j-\frac{1}{2}} - (\,\overline{\rho u}\,)_j^{\text{int}}\big) \\
&\quad - a^-_{j+\frac{1}{2}}\big((\,\overline{\rho u}\,)^{\text{int}}_{j+\frac{1}{2}} - (\,\overline{\rho u}\,)_j^{\text{int}}\big) \\
&\quad + \delta_{j-\frac{1}{2}} u^{\text{int}}_{j-\frac{1}{2}} - \delta_{j+\frac{1}{2}} u^{\text{int}}_{j+\frac{1}{2}}\Big],
\end{aligned} \tag{3.17}$$

and for E:

$$\begin{aligned}
\overline{E}_j^{\,n+1} &= \overline{E}_j^{\,\text{int}} + \frac{\Delta t^n}{\Delta x}\Big[a^+_{j-\frac{1}{2}}\big(\overline{E}^{\,\text{int,R}}_{j-\frac{1}{2}} - \overline{E}_j^{\,\text{int}}\big) - a^-_{j+\frac{1}{2}}\big(\overline{E}^{\,\text{int,L}}_{j+\frac{1}{2}} - \overline{E}_j^{\,\text{int}}\big)\Big] \\
&\overset{(3.15)}{=} \overline{E}_j^{\,\text{int}} + \frac{\Delta t^n}{\Delta x}\Big[a^+_{j-\frac{1}{2}}\big(\overline{E}^{\,\text{int}}_{j-\frac{1}{2}} - \overline{E}_j^{\,\text{int}}\big) - a^-_{j+\frac{1}{2}}\big(\overline{E}^{\,\text{int}}_{j+\frac{1}{2}} - \overline{E}_j^{\,\text{int}}\big) \\
&\quad + \frac{\delta_{j-\frac{1}{2}}}{2}\big(u^{\text{int}}_{j-\frac{1}{2}}\big)^2 - \frac{\delta_{j+\frac{1}{2}}}{2}\big(u^{\text{int}}_{j+\frac{1}{2}}\big)^2\Big].
\end{aligned} \tag{3.18}$$

We stress that the resulting fully discrete scheme (3.16)–(3.18), (2.7), (2.10), (3.14) is quite cumbersome. Moreover, it is formally first-order accurate due to the fact that it is based on a piecewise constant interpolant (2.11), (3.1). We, however, are not going to test this fully discrete scheme on any numerical examples. Instead, we will pass to the semi-discrete limit and, as explained in Remark 2.4, the use of the piecewise constant interpolant at the projection step will not affect the order of the resulting semi-discrete scheme.

3.1.2 Semi-Discrete Scheme

We now pass to the semi-discrete limit $\Delta t^n \to 0$ in (3.16). This results in

$$\begin{aligned}
\frac{\mathrm{d}}{\mathrm{d}t}\,\overline{\rho}_j(t^n) &= \lim_{\Delta t^n\to 0}\frac{\overline{\rho}_j^{\,n+1} - \overline{\rho}_j^{\,n}}{\Delta t^n} = \lim_{\Delta t^n\to 0}\frac{\overline{\rho}_j^{\,\text{int}} - \overline{\rho}_j^{\,n}}{\Delta t^n} \\
&\quad + \frac{1}{\Delta x}\Big[a^+_{j-\frac{1}{2}}\lim_{\Delta t^n\to 0}\overline{\rho}^{\,\text{int}}_{j-\frac{1}{2}} + \big(a^-_{j+\frac{1}{2}} - a^+_{j-\frac{1}{2}}\big)\lim_{\Delta t^n\to 0}\overline{\rho}_j^{\,\text{int}} - a^-_{j+\frac{1}{2}}\lim_{\Delta t^n\to 0}\overline{\rho}^{\,\text{int}}_{j+\frac{1}{2}} \\
&\quad + \lim_{\Delta t^n\to 0}(\delta_{j-\frac{1}{2}} - \delta_{j+\frac{1}{2}})\Big].
\end{aligned}$$

We then proceed as in Sect. 2.2 and end up with the following semi-discretization of the ρ equation in (3.3):

$$\frac{\mathrm{d}}{\mathrm{d}t}\,\overline{\rho}_j = -\frac{\mathcal{F}^\rho_{j+\frac{1}{2}} - \mathcal{F}^\rho_{j-\frac{1}{2}}}{\Delta x}, \tag{3.19}$$

where

$$\mathcal{F}^{\rho}_{j+\frac{1}{2}} = \frac{a^+_{j+\frac{1}{2}}(\rho u)^-_{j+\frac{1}{2}} - a^-_{j+\frac{1}{2}}(\rho u)^+_{j+\frac{1}{2}}}{a^+_{j+\frac{1}{2}} - a^-_{j+\frac{1}{2}}} + \frac{a^+_{j+\frac{1}{2}}a^-_{j+\frac{1}{2}}}{a^+_{j+\frac{1}{2}} - a^-_{j+\frac{1}{2}}}\left[\rho^+_{j+\frac{1}{2}} - \rho^-_{j+\frac{1}{2}}\right] + q_{j+\frac{1}{2}} \tag{3.20}$$

is a LDCU numerical flux with the modified "built-in" anti-diffusion term

$$\begin{aligned} q_{j+\frac{1}{2}} &= \lim_{\Delta t^n \to 0} \delta_{j+\frac{1}{2}} \\ &\overset{(3.10),\,(3.14)}{=} \lim_{\Delta t^n \to 0} \operatorname{minmod}\Big(-a^-_{j+\frac{1}{2}}\big(\overline{\rho}^{\,\text{int}}_{j+\frac{1}{2}} - \rho^{\text{int}}_{j+\frac{1}{2},\ell}\big), a^+_{j+\frac{1}{2}}\big(\rho^{\text{int}}_{j+\frac{1}{2},r} - \overline{\rho}^{\,\text{int}}_{j+\frac{1}{2}}\big)\Big) \\ &= \operatorname{minmod}\Big(-a^-_{j+\frac{1}{2}}\big(\rho^*_{j+\frac{1}{2}} - \rho^-_{j+\frac{1}{2}}\big), a^+_{j+\frac{1}{2}}\big(\rho^+_{j+\frac{1}{2}} - \rho^*_{j+\frac{1}{2}}\big)\Big), \end{aligned} \tag{3.21}$$

where $\rho^*_{j+\frac{1}{2}}$ is given by (2.20).

Similarly, we pass to the semi-discrete limit $\Delta t^n \to 0$ in (3.17) and (3.18), and proceed as in Sect. 2.2 to end up with the following semi-discretizations of the ρu and E equations in (3.3):

$$\frac{\mathrm{d}}{\mathrm{d}t}\big(\overline{\rho u}\big)_j = -\frac{\mathcal{F}^{\rho u}_{j+\frac{1}{2}} - \mathcal{F}^{\rho u}_{j-\frac{1}{2}}}{\Delta x}, \quad \frac{\mathrm{d}}{\mathrm{d}t}\,\overline{E}_{\,j} = -\frac{\mathcal{F}^{E}_{j+\frac{1}{2}} - \mathcal{F}^{E}_{j-\frac{1}{2}}}{\Delta x}, \tag{3.22}$$

where the corresponding LDCU numerical fluxes are

$$\begin{aligned} \mathcal{F}^{\rho u}_{j+\frac{1}{2}} &= \frac{a^+_{j+\frac{1}{2}}\Big[\rho^-_{j+\frac{1}{2}}\big(u^-_{j+\frac{1}{2}}\big)^2 + p^-_{j+\frac{1}{2}}\Big] - a^-_{j+\frac{1}{2}}\Big[\rho^+_{j+\frac{1}{2}}\big(u^+_{j+\frac{1}{2}}\big)^2 + p^+_{j+\frac{1}{2}}\Big]}{a^+_{j+\frac{1}{2}} - a^-_{j+\frac{1}{2}}} \\ &\quad + \frac{a^+_{j+\frac{1}{2}}a^-_{j+\frac{1}{2}}}{a^+_{j+\frac{1}{2}} - a^-_{j+\frac{1}{2}}}\left[(\rho u)^+_{j+\frac{1}{2}} - (\rho u)^-_{j+\frac{1}{2}}\right] + u^*_{j+\frac{1}{2}}q_{j+\frac{1}{2}}, \end{aligned} \tag{3.23}$$

$$\begin{aligned} \mathcal{F}^{E}_{j+\frac{1}{2}} &= \frac{a^+_{j+\frac{1}{2}}\Big[u^+_{j+\frac{1}{2}}\big(E^+_{j+\frac{1}{2}} + p^+_{j+\frac{1}{2}}\big)\Big] - a^-_{j+\frac{1}{2}}\Big[u^+_{j+\frac{1}{2}}\big(E^+_{j+\frac{1}{2}} + p^+_{j+\frac{1}{2}}\big)\Big]}{a^+_{j+\frac{1}{2}} - a^-_{j+\frac{1}{2}}} \\ &\quad + \frac{a^+_{j+\frac{1}{2}}a^-_{j+\frac{1}{2}}}{a^+_{j+\frac{1}{2}} - a^-_{j+\frac{1}{2}}}\left[E^+_{j+\frac{1}{2}} - E^-_{j+\frac{1}{2}}\right] + \frac{\big(u^*_{j+\frac{1}{2}}\big)^2}{2}q_{j+\frac{1}{2}}. \end{aligned} \tag{3.24}$$

In (3.23) and (3.24), $u^{\pm}_{j+\frac{1}{2}}$ and $p^{\pm}_{j+\frac{1}{2}}$ are given by (3.5), and in the "built-in" anti-diffusion terms on the RHS of (3.23) and (3.24), $q_{j+\frac{1}{2}}$ is given by (3.21) and $u^*_{j+\frac{1}{2}} = (\rho u)^*_{j+\frac{1}{2}}/\rho^*_{j+\frac{1}{2}}$, where $\rho^*_{j+\frac{1}{2}}$ and $(\rho u)^*_{j+\frac{1}{2}}$ are given by (2.20).

Remark 3.3 As in Sect. 2.2, the computation of the LDCU numerical fluxes in (3.20), (3.23) and (3.24) needs to be desingularized; see Remark 2.2 for details.

3.2 New LDCU Scheme for the 2-D Euler Equations of Gas Dynamics

In this section, we extend the new LDCU scheme from Sect. 3.1 to the 2-D Euler equations of gas dynamics, which read as (1.2) with

$$\boldsymbol{U}=\begin{pmatrix}\rho\\ \rho u\\ \rho v\\ E\end{pmatrix},\quad \boldsymbol{F}(\boldsymbol{U})=\begin{pmatrix}\rho u\\ \rho u^2+p\\ \rho uv\\ u(E+p)\end{pmatrix},\quad \boldsymbol{G}(\boldsymbol{U})=\begin{pmatrix}\rho v\\ \rho uv\\ \rho v^2+p\\ v(E+p)\end{pmatrix}. \tag{3.25}$$

Here, ρ is the density, u and v are the x- and y-velocities, respectively, p is the pressure, and E is the total energy. The system (1.2), (3.25) is closed using the following EOS for the ideal gas:

$$p=(\gamma-1)\Big[E-\frac{\rho}{2}(u^2+v^2)\Big],\quad \gamma=\text{Const}. \tag{3.26}$$

.

The 2-D extension of the new semi-discrete LDCU scheme (3.19)–(3.24) will be carried out in the "dimension-by-dimension" manner and the 2-D semi-discretization will read as

$$\frac{\mathrm{d}}{\mathrm{d}t}\,\overline{\boldsymbol{U}}_{\,j,k}=-\frac{\boldsymbol{\mathcal{F}}_{j+\frac12,k}-\boldsymbol{\mathcal{F}}_{j-\frac12,k}}{\Delta x}-\frac{\boldsymbol{\mathcal{G}}_{j,k+\frac12}-\boldsymbol{\mathcal{G}}_{j,k-\frac12}}{\Delta y}, \tag{3.27}$$

where $\overline{\boldsymbol{U}}_{\,j,k}:\approx\frac{1}{\Delta x\Delta y}\iint_{C_{j,k}}\boldsymbol{U}(x,y,t)\,\mathrm{d}x\mathrm{d}y$ are the computed cell averages of $\boldsymbol{U}$ over the Cartesian cells $C_{j,k}=[x_{j-\frac12},x_{j+\frac12}]\times[y_{k-\frac12},y_{k+\frac12}]$ centered at $(x_j,y_k)=((x_{j-\frac12}+x_{j+\frac12})/2,(y_{k-\frac12}+y_{k+\frac12})/2)$. For the sake of simplicity, the cells are assumed to be uniform with $x_{j+\frac12}-x_{j-\frac12}\equiv\Delta x$ and $y_{k+\frac12}-y_{k-\frac12}\equiv\Delta y$ for all j,k. In (3.27), $\boldsymbol{\mathcal{F}}_{j+\frac12,k}$ and $\boldsymbol{\mathcal{G}}_{j,k+\frac12}$ are the x- and y-numerical fluxes.

Before evaluating the numerical fluxes, we reconstruct the second-order piecewise linear interpolant

$$\widetilde{\boldsymbol{U}}(x,y)=\sum_{j,k}\Big[\,\overline{\boldsymbol{U}}_{\,j,k}+(\boldsymbol{U}_x)_{j,k}(x-x_j)+(\boldsymbol{U}_y)_{j,k}(y-y_k)\Big]\mathcal{X}_{j,k}(x,y), \tag{3.28}$$

where $\mathcal{X}_{j,k}(x,y)$ is the characteristic function of the cell $C_{j,k}$, and $(\boldsymbol{U}_x)_{j,k}$ and $(\boldsymbol{U}_y)_{j,k}$ are the slopes which are supposed to be computed using a nonlinear limiter to ensure a non-oscillatory nature of (3.28). In the numerical experiments reported in Sect. 4, we have used the generalized minmod limiter:

$$\begin{aligned}(\boldsymbol{U}_x)_{j,k}&=\text{minmod}\left(\theta\,\frac{\overline{\boldsymbol{U}}_{\,j+1,k}-\overline{\boldsymbol{U}}_{\,j,k}}{\Delta x},\ \frac{\overline{\boldsymbol{U}}_{\,j+1,k}-\overline{\boldsymbol{U}}_{\,j-1,k}}{2\Delta x},\ \theta\,\frac{\overline{\boldsymbol{U}}_{\,j,k}-\overline{\boldsymbol{U}}_{\,j-1,k}}{\Delta x}\right),\\ (\boldsymbol{U}_y)_{j,k}&=\text{minmod}\left(\theta\,\frac{\overline{\boldsymbol{U}}_{\,j,k+1}-\overline{\boldsymbol{U}}_{\,j,k}}{\Delta y},\ \frac{\overline{\boldsymbol{U}}_{\,j,k+1}-\overline{\boldsymbol{U}}_{\,j,k-1}}{2\Delta y},\ \theta\,\frac{\overline{\boldsymbol{U}}_{\,j,k}-\overline{\boldsymbol{U}}_{\,j,k-1}}{\Delta y}\right),\end{aligned}\quad \theta\in[1,2], \tag{3.29}$$

where the minmod function (2.3) is applied in a componentwise manner.

We then use the reconstruction (3.28)–(3.29) to compute the point values of $\boldsymbol{U}$ inside the cell $C_{j,k}$, which we denote by

$$\boldsymbol{U}^{-}_{j+\frac{1}{2},k} := \lim_{x\to x^{-}_{j+\frac{1}{2}}} \widetilde{\boldsymbol{U}}(x,y_k) = \overline{\boldsymbol{U}}_{j,k} + \frac{\Delta x}{2}(\boldsymbol{U}_x)_{j,k},$$

$$\boldsymbol{U}^{+}_{j+\frac{1}{2},k} := \lim_{x\to x^{+}_{j+\frac{1}{2}}} \widetilde{\boldsymbol{U}}(x,y_k) = \overline{\boldsymbol{U}}_{j+1,k} - \frac{\Delta x}{2}(\boldsymbol{U}_x)_{j+1,k},$$

$$\boldsymbol{U}^{-}_{j,k+\frac{1}{2}} := \lim_{y\to y^{-}_{k+\frac{1}{2}}} \widetilde{\boldsymbol{U}}(x_j,y) = \overline{\boldsymbol{U}}_{j,k} + \frac{\Delta y}{2}(\boldsymbol{U}_y)_{j,k},$$

$$\boldsymbol{U}^{+}_{j,k+\frac{1}{2}} := \lim_{y\to y^{+}_{k+\frac{1}{2}}} \widetilde{\boldsymbol{U}}(x_j,y) = \overline{\boldsymbol{U}}_{j,k+1} - \frac{\Delta y}{2}(\boldsymbol{U}_y)_{j,k+1}.$$

We now develop the LDCU numerical fluxes $\boldsymbol{\mathcal{F}}_{j+\frac{1}{2},k}$ and $\boldsymbol{\mathcal{G}}_{j,k+\frac{1}{2}}$ using the "dimension-by-dimension" approach. To this end, $\boldsymbol{\mathcal{F}}_{j+\frac{1}{2},k}$ is designed by considering the 1-D restrictions of the system (1.2), (3.25) along the lines $y = y_k$:

$$\boldsymbol{U}_t(x,y_k,t) + \boldsymbol{F}\big(\boldsymbol{U}(x,y_k,t)\big)_x = \boldsymbol{0}. \tag{3.30}$$

Similarly, in order to design $\boldsymbol{\mathcal{G}}_{j,k+\frac{1}{2}}$ one needs to consider the 1-D restrictions of (1.2), (3.25) along the lines $x = x_j$:

$$\boldsymbol{U}_t(x_j,y,t) + \boldsymbol{G}\big(\boldsymbol{U}(x_j,y,t)\big)_y = \boldsymbol{0}.$$

Notice that the 1-D systems in (3.30) do not coincide with the original 1-D Euler equation of gas dynamics (1.1), (3.3), as (3.30) has an additional equation

$$(\rho v)_t + (\rho u v)_x = 0,$$

which is, in fact, just a transport equation for ρv. Therefore, when an isolated contact wave propagates in the x-direction along $y = y_k$, ρv will jump across the contact wave similarly to ρ. This helps us to extend the construction of the subcell averages $\overline{\boldsymbol{U}}^{\,\text{int,L}}$ and $\overline{\boldsymbol{U}}^{\,\text{int,R}}$ introduced in §3.1 to the quasi 1-D case considered here.

Recall that the 1-D LDCU fluxes (3.20), (3.23), and (3.24) have been derived through the fully discrete framework. Therefore, we have to go through the quasi 1-D fully discrete scheme derivation for the systems in (3.30). To this end, we follow all of the steps in §2.1 and §3.1 and we now focus on the details, which are different from what has been done there.

First, (3.1) now reads as

$$\widetilde{\boldsymbol{U}}^{\,\text{int}}_{j+\frac{1}{2},k}(x,y_k) = \begin{cases} \overline{\boldsymbol{U}}^{\,\text{int,L}}_{j+\frac{1}{2},k}, & x < x_{j+\frac{1}{2}}, \\ \overline{\boldsymbol{U}}^{\,\text{int,R}}_{j+\frac{1}{2},k}, & x > x_{j+\frac{1}{2}}, \end{cases}$$

and the conservation requirements (3.2), which become

$$a^{+}_{j+\frac{1}{2},k}\,\overline{\boldsymbol{U}}^{\,\text{int,R}}_{j+\frac{1}{2},k} - a^{-}_{j+\frac{1}{2},k}\,\overline{\boldsymbol{U}}^{\,\text{int,L}}_{j+\frac{1}{2},k} = \big(a^{+}_{j+\frac{1}{2},k} - a^{-}_{j+\frac{1}{2},k}\big)\,\overline{\boldsymbol{U}}^{\,\text{int}}_{j+\frac{1}{2},k}, \tag{3.31}$$

are still valid with $a^{\pm}_{j+\frac{1}{2},k}$ being the one-sided local speeds of propagation in the x-direction along $y = y_k$. These speeds can be estimated using the eigenvalues $\lambda_1(\boldsymbol{U}) < \cdots < \lambda_4(\boldsymbol{U})$ of the Jacobian $\frac{\partial \boldsymbol{F}}{\partial \boldsymbol{U}}$ as follows:

$$a^{-}_{j+\frac{1}{2},k} := \min\left\{u^{-}_{j+\frac{1}{2},k} - c^{-}_{j+\frac{1}{2},k},\, u^{-}_{j+\frac{1}{2},k} - c^{-}_{j+\frac{1}{2},k},\, 0\right\},$$
$$a^{+}_{j+\frac{1}{2},k} := \max\left\{u^{+}_{j+\frac{1}{2},k} + c^{+}_{j+\frac{1}{2},k},\, u^{+}_{j+\frac{1}{2},k} + c^{+}_{j+\frac{1}{2},k},\, 0\right\},$$

where

$$u^{\pm}_{j+\frac{1}{2},k} = \frac{(\rho u)^{\pm}_{j+\frac{1}{2},k}}{\rho^{\pm}_{j+\frac{1}{2},k}}, \quad v^{\pm}_{j+\frac{1}{2},k} = \frac{(\rho v)^{\pm}_{j+\frac{1}{2},k}}{\rho^{\pm}_{j+\frac{1}{2},k}},$$

$$p^{\pm}_{j+\frac{1}{2},k} = (\gamma-1)\left[E^{\pm}_{j+\frac{1}{2},k} - \frac{\rho^{\pm}_{j+\frac{1}{2},k}}{2}\left(\left(u^{\pm}_{j+\frac{1}{2},k}\right)^2 + \left(v^{\pm}_{j+\frac{1}{2},k}\right)^2\right)\right], \quad c^{\pm}_{j+\frac{1}{2},k} = \sqrt{\frac{\gamma\, p^{\pm}_{j+\frac{1}{2},k}}{\rho^{\pm}_{j+\frac{1}{2},k}}}.$$

In addition to the four conservation constraints given by (3.31), we will enforce the continuity of u and p across the cell interfaces $x = x_{j+\frac{1}{2}}$ by setting

$$\frac{(\,\overline{\rho u}\,)^{\mathrm{int,L}}_{j+\frac{1}{2},k}}{\overline{\rho}^{\,\mathrm{int,L}}_{j+\frac{1}{2},k}} = \frac{(\,\overline{\rho u}\,)^{\mathrm{int,R}}_{j+\frac{1}{2},k}}{\overline{\rho}^{\,\mathrm{int,R}}_{j+\frac{1}{2},k}},$$
$$\overline{E}^{\,\mathrm{int,L}}_{j+\frac{1}{2},k} - \frac{\left((\,\overline{\rho u}\,)^{\mathrm{int,L}}_{j+\frac{1}{2},k}\right)^2 + \left((\,\overline{\rho v}\,)^{\mathrm{int,L}}_{j+\frac{1}{2},k}\right)^2}{2\,\overline{\rho}^{\,\mathrm{int,L}}_{j+\frac{1}{2},k}}$$
$$= \overline{E}^{\,\mathrm{int,R}}_{j+\frac{1}{2},k} - \frac{\left((\,\overline{\rho u}\,)^{\mathrm{int,R}}_{j+\frac{1}{2},k}\right)^2 + \left((\,\overline{\rho v}\,)^{\mathrm{int,R}}_{j+\frac{1}{2},k}\right)^2}{2\,\overline{\rho}^{\,\mathrm{int,R}}_{j+\frac{1}{2},k}},$$

and then proceed as in Algorithm 3.1 to obtain the formulae analogous to (3.10), (3.14) for both the ρ - and ρv-components:

$$\begin{aligned}
\overline{\rho}^{\,\mathrm{int,L}}_{j+\frac{1}{2},k} &= \overline{\rho}^{\,\mathrm{int}}_{j+\frac{1}{2},k} + \frac{\delta^{\rho}_{j+\frac{1}{2},k}}{a^{-}_{j+\frac{1}{2},k}}, & \overline{\rho}^{\,\mathrm{int,R}}_{j+\frac{1}{2},k} &= \overline{\rho}^{\,\mathrm{int}}_{j+\frac{1}{2},k} + \frac{\delta^{\rho}_{j+\frac{1}{2},k}}{a^{+}_{j+\frac{1}{2},k}},\\
(\,\overline{\rho v}\,)^{\mathrm{int,L}}_{j+\frac{1}{2},k} &= (\,\overline{\rho v}\,)^{\mathrm{int}}_{j+\frac{1}{2},k} + \frac{\delta^{\rho v}_{j+\frac{1}{2},k}}{a^{-}_{j+\frac{1}{2},k}}, & (\,\overline{\rho v}\,)^{\mathrm{int,R}}_{j+\frac{1}{2},k} &= (\,\overline{\rho v}\,)^{\mathrm{int}}_{j+\frac{1}{2},k} + \frac{\delta^{\rho v}_{j+\frac{1}{2},k}}{a^{+}_{j+\frac{1}{2},k}},
\end{aligned} \tag{3.32}$$

where

$$\delta^{\rho}_{j+\frac{1}{2},k} = \mathrm{minmod}\left(-a^{-}_{j+\frac{1}{2},k}\left[\,\overline{\rho}^{\,\mathrm{int}}_{j+\frac{1}{2},k} - \left(\rho^{\mathrm{int}}_{j+\frac{1}{2},k}\right)_{\ell}\right],\, a^{+}_{j+\frac{1}{2},k}\left[\left(\rho^{\mathrm{int}}_{j+\frac{1}{2},k}\right)_{r} - \overline{\rho}^{\,\mathrm{int}}_{j+\frac{1}{2},k}\right]\right),$$
$$\delta^{\rho v}_{j+\frac{1}{2},k} = \mathrm{minmod}\left(-a^{-}_{j+\frac{1}{2},k}\left[(\,\overline{\rho v}\,)^{\mathrm{int}}_{j+\frac{1}{2},k} - \left((\rho v)^{\mathrm{int}}_{j+\frac{1}{2},k}\right)_{\ell}\right],\, a^{+}_{j+\frac{1}{2},k}\left[\left((\rho v)^{\mathrm{int}}_{j+\frac{1}{2},k}\right)_{r} - (\,\overline{\rho v}\,)^{\mathrm{int}}_{j+\frac{1}{2},k}\right]\right).$$

Here, the values $\left(\rho^{\text{int}}_{j+\frac{1}{2},k}\right)_\ell$, $\left(\rho^{\text{int}}_{j+\frac{1}{2},k}\right)_r$, $\left((\rho v)^{\text{int}}_{j+\frac{1}{2},k}\right)_\ell$, and $\left((\rho v)^{\text{int}}_{j+\frac{1}{2},k}\right)_r$ are obtained using the Taylor expansions as it was done in (2.14).

We then proceed as in §3.1.2 and end up with the LDCU numerical fluxes for the first three components ρ, ρu, and ρv. The ρ - and (ρv)-fluxes are similar to (3.20) and they are

$$\begin{aligned}
\mathcal{F}^{\rho}_{j+\frac{1}{2},k} &= \frac{a^+_{j+\frac{1}{2},k}(\rho u)^-_{j+\frac{1}{2},k} - a^-_{j+\frac{1}{2},k}(\rho u)^+_{j+\frac{1}{2},k}}{a^+_{j+\frac{1}{2},k} - a^-_{j+\frac{1}{2},k}} + \frac{a^+_{j+\frac{1}{2},k}a^-_{j+\frac{1}{2},k}}{a^+_{j+\frac{1}{2},k} - a^-_{j+\frac{1}{2},k}}\left[\rho^+_{j+\frac{1}{2},k} - \rho^-_{j+\frac{1}{2},k}\right] \\
&\quad + q^{\rho}_{j+\frac{1}{2},k}, \\
\mathcal{F}^{\rho v}_{j+\frac{1}{2},k} &= \frac{a^+_{j+\frac{1}{2},k}\rho^-_{j+\frac{1}{2},k}u^-_{j+\frac{1}{2},k}v^-_{j+\frac{1}{2},k} - a^-_{j+\frac{1}{2},k}\rho^+_{j+\frac{1}{2},k}u^+_{j+\frac{1}{2},k}v^+_{j+\frac{1}{2},k}}{a^+_{j+\frac{1}{2},k} - a^-_{j+\frac{1}{2},k}} \\
&\quad + \frac{a^+_{j+\frac{1}{2},k}a^-_{j+\frac{1}{2},k}}{a^+_{j+\frac{1}{2},k} - a^-_{j+\frac{1}{2},k}}\left[(\rho v)^+_{j+\frac{1}{2},k} - (\rho v)^-_{j+\frac{1}{2},k}\right] + q^{\rho v}_{j+\frac{1}{2},k},
\end{aligned} \tag{3.33}$$

while the ρu-fluxes are similar to (3.23) and they are

$$\begin{aligned}
\mathcal{F}^{\rho u}_{j+\frac{1}{2},k} &= \frac{a^+_{j+\frac{1}{2},k}\left[\rho^-_{j+\frac{1}{2},k}\left(u^-_{j+\frac{1}{2},k}\right)^2 + p^-_{j+\frac{1}{2},k}\right] - a^-_{j+\frac{1}{2},k}\left[\rho^+_{j+\frac{1}{2},k}\left(u^+_{j+\frac{1}{2},k}\right)^2 + p^+_{j+\frac{1}{2},k}\right]}{a^+_{j+\frac{1}{2},k} - a^-_{j+\frac{1}{2},k}} \\
&\quad + \frac{a^+_{j+\frac{1}{2},k}a^-_{j+\frac{1}{2},k}}{a^+_{j+\frac{1}{2},k} - a^-_{j+\frac{1}{2},k}}\left[(\rho u)^+_{j+\frac{1}{2},k} - (\rho u)^-_{j+\frac{1}{2},k}\right] + u^*_{j+\frac{1}{2},k}q^{\rho}_{j+\frac{1}{2},k},
\end{aligned} \tag{3.34}$$

In (3.33) and (3.34),

$$\begin{aligned}
(\rho u)^*_{j+\frac{1}{2},k} &= \frac{a^+_{j+\frac{1}{2},k}(\rho u)^+_{j+\frac{1}{2},k} - a^-_{j+\frac{1}{2},k}(\rho u)^-_{j+\frac{1}{2},k}}{a^+_{j+\frac{1}{2},k} - a^-_{j+\frac{1}{2},k}} \\
&\quad - \frac{\left[\rho^+_{j+\frac{1}{2},k}\left(u^+_{j+\frac{1}{2},k}\right)^2 + p^+_{j+\frac{1}{2},k}\right] - \left[\rho^-_{j+\frac{1}{2},k}\left(u^-_{j+\frac{1}{2},k}\right)^2 + p^-_{j+\frac{1}{2},k}\right]}{a^+_{j+\frac{1}{2},k} - a^-_{j+\frac{1}{2},k}}, \\
\rho^*_{j+\frac{1}{2},k} &= \frac{a^+_{j+\frac{1}{2},k}\rho^+_{j+\frac{1}{2},k} - a^-_{j+\frac{1}{2},k}\rho^-_{j+\frac{1}{2},k} - \left\{(\rho u)^+_{j+\frac{1}{2},k} - (\rho u)^-_{j+\frac{1}{2},k}\right\}}{a^+_{j+\frac{1}{2},k} - a^-_{j+\frac{1}{2},k}}, \\
u^*_{j+\frac{1}{2},k} &= \frac{(\rho u)^*_{j+\frac{1}{2},k}}{\rho^*_{j+\frac{1}{2},k}},
\end{aligned}$$

and

$$\begin{aligned}
q^{\rho}_{j+\frac{1}{2},k} &= \text{minmod}\left(-a^-_{j+\frac{1}{2},k}\left(\rho^*_{j+\frac{1}{2},k} - \rho^-_{j+\frac{1}{2},k}\right),\ a^+_{j+\frac{1}{2},k}\left(\rho^+_{j+\frac{1}{2},k} - \rho^*_{j+\frac{1}{2},k}\right)\right), \\
q^{\rho v}_{j+\frac{1}{2},k} &= \text{minmod}\left(-a^-_{j+\frac{1}{2},k}\left((\rho v)^*_{j+\frac{1}{2},k} - (\rho v)^-_{j+\frac{1}{2},k}\right),\ a^+_{j+\frac{1}{2},k}\left((\rho v)^+_{j+\frac{1}{2},k} - (\rho v)^*_{j+\frac{1}{2},k}\right)\right),
\end{aligned}$$

where

$$(\rho v)^*_{j+\frac{1}{2},k} = \frac{a^+_{j+\frac{1}{2},k}(\rho v)^+_{j+\frac{1}{2},k} - a^-_{j+\frac{1}{2},k}(\rho v)^-_{j+\frac{1}{2},k} - \left\{\rho^+_{j+\frac{1}{2},k}u^+_{j+\frac{1}{2},k}v^+_{j+\frac{1}{2},k} - \rho^-_{j+\frac{1}{2},k}u^-_{j+\frac{1}{2},k}v^-_{j+\frac{1}{2},k}\right\}}{a^+_{j+\frac{1}{2},k} - a^-_{j+\frac{1}{2},k}}.$$

The LDCU numerical fluxes for the fourth component are, however, different from (3.24) since in the 2-D case, the EOS (3.26) contains the ρv variable. In order to derive $\mathcal{F}^E_{j+\frac{1}{2},k}$, we first write down the 2-D analogue of (3.18):

$$\begin{aligned}\overline{E}^{\,n+1}_{j,k} = \overline{E}^{\,\text{int}}_{j,k} + \frac{\Delta t^n}{\Delta x}\Bigg[& a^+_{j-\frac{1}{2},k}\left(\overline{E}^{\,\text{int,R}}_{j-\frac{1}{2},k} - \overline{E}^{\,\text{int}}_{j,k}\right) - a^-_{j+\frac{1}{2}}\left(\overline{E}^{\,\text{int,L}}_{j+\frac{1}{2},k} - \overline{E}^{\,\text{int}}_{j,k}\right) \\ & + \frac{\delta^\rho_{j-\frac{1}{2},k}}{2}\left(u^{\text{int}}_{j-\frac{1}{2},k}\right)^2 - \frac{\delta^\rho_{j+\frac{1}{2},k}}{2}\left(u^{\text{int}}_{j+\frac{1}{2},k}\right)^2 \\ & + \frac{a^+_{j+\frac{1}{2},k}a^-_{j+\frac{1}{2},k}}{a^+_{j+\frac{1}{2},k} - a^-_{j+\frac{1}{2},k}}\left\{\frac{\left(\left(\overline{\rho v}\right)^{\text{int,R}}_{j+\frac{1}{2},k}\right)^2}{2\,\overline{\rho}^{\,\text{int,R}}_{j+\frac{1}{2},k}} - \frac{\left(\left(\overline{\rho v}\right)^{\text{int,L}}_{j+\frac{1}{2},k}\right)^2}{2\,\overline{\rho}^{\,\text{int,L}}_{j+\frac{1}{2},k}}\right\} \\ & - \frac{a^+_{j-\frac{1}{2},k}a^-_{j-\frac{1}{2},k}}{a^+_{j-\frac{1}{2},k} - a^-_{j-\frac{1}{2},k}}\left\{\frac{\left(\left(\overline{\rho v}\right)^{\text{int,R}}_{j-\frac{1}{2},k}\right)^2}{2\,\overline{\rho}^{\,\text{int,R}}_{j-\frac{1}{2},k}} - \frac{\left(\left(\overline{\rho v}\right)^{\text{int,L}}_{j-\frac{1}{2},k}\right)^2}{2\,\overline{\rho}^{\,\text{int,L}}_{j-\frac{1}{2},k}}\right\}\Bigg],\end{aligned} \tag{3.35}$$

where $u^{\text{int}}_{j\pm\frac{1}{2},k} = \overline{\rho u}^{\,\text{int}}_{j\pm\frac{1}{2},k} / \overline{\rho}^{\,\text{int}}_{j\pm\frac{1}{2},k}$ and the last two terms reflect the contribution of the ρv variable. We then substitute (3.32) into (3.35) to obtain

$$\begin{aligned}\overline{E}^{\,n+1}_{j,k} = \overline{E}^{\,\text{int}}_{j,k} + \frac{\Delta t^n}{\Delta x}\Bigg[& a^+_{j-\frac{1}{2},k}\left(\overline{E}^{\,\text{int}}_{j-\frac{1}{2},k} - \overline{E}^{\,\text{int}}_{j,k}\right) - a^-_{j+\frac{1}{2}}\left(\overline{E}^{\,\text{int}}_{j+\frac{1}{2},k} - \overline{E}^{\,\text{int}}_{j,k}\right) \\ & + \frac{\delta^\rho_{j-\frac{1}{2},k}}{2}\left(u^{\text{int}}_{j-\frac{1}{2},k}\right)^2 - \frac{\delta^\rho_{j+\frac{1}{2},k}}{2}\left(u^{\text{int}}_{j+\frac{1}{2},k}\right)^2 \\ & + \frac{a^+_{j+\frac{1}{2},k}a^-_{j+\frac{1}{2},k}}{a^+_{j+\frac{1}{2},k} - a^-_{j+\frac{1}{2},k}}\left\{\frac{\left(\left(\overline{\rho v}\right)^{\text{int}}_{j+\frac{1}{2},k} + \dfrac{\delta^{\rho v}_{j+\frac{1}{2},k}}{a^+_{j+\frac{1}{2},k}}\right)^2}{2\left(\overline{\rho}^{\,\text{int}}_{j+\frac{1}{2},k} + \dfrac{\delta^\rho_{j+\frac{1}{2},k}}{a^+_{j+\frac{1}{2},k}}\right)} - \frac{\left(\left(\overline{\rho v}\right)^{\text{int}}_{j+\frac{1}{2},k} + \dfrac{\delta^{\rho v}_{j+\frac{1}{2},k}}{a^-_{j+\frac{1}{2},k}}\right)^2}{2\left(\overline{\rho}^{\,\text{int}}_{j+\frac{1}{2},k} + \dfrac{\delta^\rho_{j+\frac{1}{2},k}}{a^-_{j+\frac{1}{2},k}}\right)}\right\} \\ & - \frac{a^+_{j-\frac{1}{2},k}a^-_{j-\frac{1}{2},k}}{a^+_{j-\frac{1}{2},k} - a^-_{j-\frac{1}{2},k}}\left\{\frac{\left(\left(\overline{\rho v}\right)^{\text{int}}_{j-\frac{1}{2},k} + \dfrac{\delta^{\rho v}_{j-\frac{1}{2},k}}{a^+_{j-\frac{1}{2},k}}\right)^2}{2\left(\overline{\rho}^{\,\text{int}}_{j-\frac{1}{2},k} + \dfrac{\delta^\rho_{j-\frac{1}{2},k}}{a^+_{j-\frac{1}{2},k}}\right)} - \frac{\left(\left(\overline{\rho v}\right)^{\text{int}}_{j-\frac{1}{2},k} + \dfrac{\delta^{\rho v}_{j-\frac{1}{2},k}}{a^-_{j-\frac{1}{2},k}}\right)^2}{2\left(\overline{\rho}^{\,\text{int}}_{j-\frac{1}{2},k} + \dfrac{\delta^\rho_{j-\frac{1}{2},k}}{a^-_{j-\frac{1}{2},k}}\right)}\right\}\Bigg],\end{aligned}$$

and pass to the semi-discrete limit $\Delta t^n \to 0$ as in §3.1 to end up with

$$\mathcal{F}^E_{j+\frac{1}{2},k} = \frac{a^+_{j+\frac{1}{2},k}u^-_{j+\frac{1}{2},k}\left(E^-_{j+\frac{1}{2},k}+p^-_{j+\frac{1}{2},k}\right)-a^-_{j+\frac{1}{2},k}u^+_{j+\frac{1}{2},k}\left(E^+_{j+\frac{1}{2},k}+p^+_{j+\frac{1}{2},k}\right)}{a^+_{j+\frac{1}{2},k}-a^-_{j+\frac{1}{2},k}}$$
$$+\frac{a^+_{j+\frac{1}{2},k}a^-_{j+\frac{1}{2},k}}{a^+_{j+\frac{1}{2},k}-a^-_{j+\frac{1}{2},k}}\left[E^+_{j+\frac{1}{2},k}-E^-_{j+\frac{1}{2},k}-\frac{\left((\rho v)^*_{j+\frac{1}{2},k}+\dfrac{q^{\rho v}_{j+\frac{1}{2},k}}{a^+_{j+\frac{1}{2},k}}\right)^2}{2\left(\rho^*_{j+\frac{1}{2},k}+\dfrac{q^{\rho}_{j+\frac{1}{2},k}}{a^+_{j+\frac{1}{2},k}}\right)}\right.$$
$$\left.+\frac{\left((\rho v)^*_{j+\frac{1}{2},k}+\dfrac{q^{\rho v}_{j+\frac{1}{2},k}}{a^-_{j+\frac{1}{2},k}}\right)^2}{2\left(\rho^*_{j+\frac{1}{2},k}+\dfrac{q^{\rho}_{j+\frac{1}{2},k}}{a^-_{j+\frac{1}{2},k}}\right)}\right]+\frac{\left(u^*_{j+\frac{1}{2},k}\right)^2}{2}q^{\rho}_{j+\frac{1}{2},k}. \tag{3.36}$$

The LDCU numerical fluxes in the y-direction are obtained in a similar way and they are given by

$$\mathcal{G}^{\rho}_{j,k+\frac{1}{2}} = \frac{b^+_{j,k+\frac{1}{2}}(\rho u)^-_{j,k+\frac{1}{2}}-b^-_{j,k+\frac{1}{2}}(\rho u)^+_{j,k+\frac{1}{2}}}{b^+_{j,k+\frac{1}{2}}-b^-_{j,k+\frac{1}{2}}}+\frac{b^+_{j,k+\frac{1}{2}}b^-_{j,k+\frac{1}{2}}}{b^+_{j,k+\frac{1}{2}}-b^-_{j,k+\frac{1}{2}}}\left[\rho^+_{j,k+\frac{1}{2}}-\rho^-_{j,k+\frac{1}{2}}\right]$$
$$+q^{\rho}_{j,k+\frac{1}{2}},$$
$$\mathcal{G}^{\rho u}_{j,k+\frac{1}{2}} = \frac{b^+_{j,k+\frac{1}{2}}\rho^-_{j,k+\frac{1}{2}}u^-_{j,k+\frac{1}{2}}v^-_{j,k+\frac{1}{2}}-b^-_{j,k+\frac{1}{2}}\rho^+_{j,k+\frac{1}{2}}u^+_{j,k+\frac{1}{2}}v^+_{j,k+\frac{1}{2}}}{b^+_{j,k+\frac{1}{2}}-b^-_{j,k+\frac{1}{2}}}$$
$$+\frac{b^+_{j,k+\frac{1}{2}}b^-_{j,k+\frac{1}{2}}}{b^+_{j,k+\frac{1}{2}}-b^-_{j,k+\frac{1}{2}}}\left[(\rho u)^+_{j,k+\frac{1}{2}}-(\rho u)^-_{j,k+\frac{1}{2}}\right]+q^{\rho u}_{j,k+\frac{1}{2}},$$
$$\mathcal{G}^{\rho v}_{j,k+\frac{1}{2}} = \frac{b^+_{j,k+\frac{1}{2}}\left[\rho^-_{j,k+\frac{1}{2}}\left(v^-_{j,k+\frac{1}{2}}\right)^2+p^-_{j,k+\frac{1}{2}}\right]-b^-_{j,k+\frac{1}{2}}\left[\rho^+_{j,k+\frac{1}{2}}\left(v^+_{j,k+\frac{1}{2}}\right)^2+p^+_{j,k+\frac{1}{2}}\right]}{b^+_{j,k+\frac{1}{2}}-b^-_{j,k+\frac{1}{2}}}$$
$$+\frac{b^+_{j,k+\frac{1}{2}}b^-_{j,k+\frac{1}{2}}}{b^+_{j,k+\frac{1}{2}}-b^-_{j,k+\frac{1}{2}}}\left[(\rho v)^+_{j,k+\frac{1}{2}}-(\rho v)^-_{j,k+\frac{1}{2}}\right]+v^*_{j,k+\frac{1}{2}}q^{\rho}_{j,k+\frac{1}{2}},$$
$$\mathcal{G}^{E}_{j,k+\frac{1}{2}} = \frac{b^+_{j,k+\frac{1}{2}}v^-_{j,k+\frac{1}{2}}\left(E^-_{j,k+\frac{1}{2}}+p^-_{j,k+\frac{1}{2}}\right)-b^-_{j,k+\frac{1}{2}}v^+_{j,k+\frac{1}{2}}\left(E^+_{j,k+\frac{1}{2}}+p^+_{j,k+\frac{1}{2}}\right)}{b^+_{j,k+\frac{1}{2}}-b^-_{j,k+\frac{1}{2}}}$$

$$+\frac{b^+_{j,k+\frac{1}{2}}b^-_{j,k+\frac{1}{2}}}{b^+_{j,k+\frac{1}{2}}-b^-_{j,k+\frac{1}{2}}}\left[E^+_{j,k+\frac{1}{2}}-E^-_{j,k+\frac{1}{2}}-\frac{\left((\rho u)^*_{j,k+\frac{1}{2}}+\frac{q^{\rho u}_{j,k+\frac{1}{2}}}{b^+_{j,k+\frac{1}{2}}}\right)^2}{2\left(\rho^*_{j,k+\frac{1}{2}}+\frac{q^{\rho}_{j,k+\frac{1}{2}}}{b^+_{j,k+\frac{1}{2}}}\right)}\right.$$
$$\left.+\frac{\left((\rho u)^*_{j,k+\frac{1}{2}}+\frac{q^{\rho u}_{j,k+\frac{1}{2}}}{b^-_{j,k+\frac{1}{2}}}\right)^2}{2\left(\rho^*_{j,k+\frac{1}{2}}+\frac{q^{\rho}_{j,k+\frac{1}{2}}}{b^-_{j,k+\frac{1}{2}}}\right)}\right]+\frac{\left(v^*_{j,k+\frac{1}{2}}\right)^2}{2}q^{\rho}_{j,k+\frac{1}{2}}. \tag{3.37}$$

Here, $b^{\pm}_{j,k+\frac{1}{2}}$ are the one-sided local speeds of propagation in the y-direction along the line $x = x_j$. These speeds can be estimated using the eigenvalues $\mu_1(\boldsymbol{U}) < \cdots < \mu_4(\boldsymbol{U})$ of the Jacobian $\frac{\partial \boldsymbol{G}}{\partial \boldsymbol{U}}$ as follows:

$$b^-_{j,k+\frac{1}{2}} := \min\left\{v^-_{j,k+\frac{1}{2}}-c^-_{j,k+\frac{1}{2}},\ v^-_{j,k+\frac{1}{2}}-c^-_{j,k+\frac{1}{2}},\ 0\right\},$$
$$b^+_{j,k+\frac{1}{2}} := \max\left\{v^+_{j,k+\frac{1}{2}}+c^+_{j,k+\frac{1}{2}},\ v^+_{j,k+\frac{1}{2}}+c^+_{j,k+\frac{1}{2}},\ 0\right\},$$

where

$$u^{\pm}_{j,k+\frac{1}{2}}=\frac{(\rho u)^{\pm}_{j,k+\frac{1}{2}}}{\rho^{\pm}_{j,k+\frac{1}{2}}},\quad v^{\pm}_{j,k+\frac{1}{2}}=\frac{(\rho v)^{\pm}_{j,k+\frac{1}{2}}}{\rho^{\pm}_{j,k+\frac{1}{2}}},$$
$$p^{\pm}_{j,k+\frac{1}{2}}=(\gamma-1)\left[E^{\pm}_{j,k+\frac{1}{2}}-\frac{\rho^{\pm}_{j,k+\frac{1}{2}}}{2}\left((u^{\pm}_{j,k+\frac{1}{2}})^2+(v^{\pm}_{j,k+\frac{1}{2}})^2\right)\right],$$
$$c^{\pm}_{j,k+\frac{1}{2}}=\sqrt{\frac{\gamma p^{\pm}_{j,k+\frac{1}{2}}}{\rho^{\pm}_{j,k+\frac{1}{2}}}},$$
$$(\rho v)^*_{j,k+\frac{1}{2}}=\frac{b^+_{j,k+\frac{1}{2}}(\rho v)^+_{j,k+\frac{1}{2}}-b^-_{j,k+\frac{1}{2}}(\rho v)^-_{j,k+\frac{1}{2}}}{b^+_{j,k+\frac{1}{2}}-b^-_{j,k+\frac{1}{2}}}$$
$$-\frac{\left[\rho^+_{j,k+\frac{1}{2}}(v^+_{j,k+\frac{1}{2}})^2+p^+_{j,k+\frac{1}{2}}\right]-\left[\rho^-_{j,k+\frac{1}{2}}(v^-_{j,k+\frac{1}{2}})^2+p^-_{j,k+\frac{1}{2}}\right]}{b^+_{j,k+\frac{1}{2}}-b^-_{j,k+\frac{1}{2}}},$$
$$\rho^*_{j,k+\frac{1}{2}}=\frac{b^+_{j,k+\frac{1}{2}}\rho^+_{j,k+\frac{1}{2}}-b^-_{j,k+\frac{1}{2}}\rho^-_{j,k+\frac{1}{2}}-\left\{(\rho v)^+_{j,k+\frac{1}{2}}-(\rho v)^-_{j,k+\frac{1}{2}}\right\}}{b^+_{j,k+\frac{1}{2}}-b^-_{j,k+\frac{1}{2}}},$$
$$v^*_{j,k+\frac{1}{2}}=\frac{(\rho v)^*_{j,k+\frac{1}{2}}}{\rho^*_{j,k+\frac{1}{2}}},$$

$$(\rho u)^*_{j,k+\frac{1}{2}} = \frac{b^+_{j,k+\frac{1}{2}}(\rho u)^+_{j,k+\frac{1}{2}} - b^-_{j,k+\frac{1}{2}}(\rho u)^-_{j,k+\frac{1}{2}} - \left\{\rho^+_{j,k+\frac{1}{2}} u^+_{j,k+\frac{1}{2}} v^+_{j,k+\frac{1}{2}} - \rho^-_{j,k+\frac{1}{2}} u^-_{j,k+\frac{1}{2}} v^-_{j,k+\frac{1}{2}}\right\}}{b^+_{j,k+\frac{1}{2}} - b^-_{j,k+\frac{1}{2}}},$$

$$q^{\rho}_{j,k+\frac{1}{2}} = \text{minmod}\left(-b^-_{j,k+\frac{1}{2}}\left(\rho^*_{j,k+\frac{1}{2}} - \rho^-_{j,k+\frac{1}{2}}\right),\ b^+_{j,k+\frac{1}{2}}\left(\rho^+_{j,k+\frac{1}{2}} - \rho^*_{j,k+\frac{1}{2}}\right)\right),$$

$$q^{\rho u}_{j,k+\frac{1}{2}} = \text{minmod}\left(-b^-_{j,k+\frac{1}{2}}\left((\rho u)^*_{j,k+\frac{1}{2}} - (\rho u)^-_{j,k+\frac{1}{2}}\right),\ b^+_{j,k+\frac{1}{2}}\left((\rho u)^+_{j,k+\frac{1}{2}} - (\rho u)^*_{j,k+\frac{1}{2}}\right)\right).$$

Remark 3.4 We note that as in the 1-D case, the computation of the LDCU numerical fluxes needs to be desingularized. In particular, if $a^+_{j+\frac{1}{2},k} < \varepsilon$ and $a^-_{j+\frac{1}{2},k} > -\varepsilon$ for a small positive ε, we replace the x-numerical fluxes with

$$\mathcal{F}_{j+\frac{1}{2},k} = \frac{\boldsymbol{F}\left(\boldsymbol{U}^-_{j+\frac{1}{2},k}\right) + \boldsymbol{F}\left(\boldsymbol{U}^+_{j+\frac{1}{2},k}\right)}{2}.$$

Similarly, if $b^+_{j,k+\frac{1}{2}} < \varepsilon$ and $b^-_{j,k+\frac{1}{2}} > -\varepsilon$, we replace the y-numerical fluxes with

$$\mathcal{G}_{j,k+\frac{1}{2}} = \frac{\boldsymbol{G}\left(\boldsymbol{U}^-_{j,k+\frac{1}{2}}\right) + \boldsymbol{G}\left(\boldsymbol{U}^+_{j,k+\frac{1}{2}}\right)}{2}.$$

In addition, the computation of the energy numerical fluxes (3.36) and (3.37) have to be desingularized even in the case when only one of the local speeds is very small. In particular,

$$\begin{aligned}
&\text{if } a^+_{j+\frac{1}{2},k} < \varepsilon \text{ but } a^-_{j+\frac{1}{2},k} < -\varepsilon, \quad \text{we take } \mathcal{F}^E_{j+\frac{1}{2},k} = u^-_{j+\frac{1}{2},k}\left(E^-_{j+\frac{1}{2},k} + p^-_{j+\frac{1}{2},k}\right);\\
&\text{if } a^-_{j+\frac{1}{2},k} > -\varepsilon \text{ but } a^+_{j+\frac{1}{2},k} > \varepsilon, \quad \text{we take } \mathcal{F}^E_{j+\frac{1}{2},k} = u^+_{j+\frac{1}{2},k}\left(E^+_{j+\frac{1}{2},k} + p^+_{j+\frac{1}{2},k}\right);\\
&\text{if } b^+_{j,k+\frac{1}{2}} < \varepsilon \text{ but } b^-_{j,k+\frac{1}{2}} < -\varepsilon, \quad \text{we take } \mathcal{G}^E_{j,k+\frac{1}{2}} = v^-_{j,k+\frac{1}{2}}\left(E^-_{j,k+\frac{1}{2}} + p^-_{j,k+\frac{1}{2}}\right);\\
&\text{if } b^-_{j,k+\frac{1}{2}} > -\varepsilon \text{ but } b^+_{j,k+\frac{1}{2}} > \varepsilon, \quad \text{we take } \mathcal{G}^E_{j,k+\frac{1}{2}} = v^+_{j,k+\frac{1}{2}}\left(E^+_{j,k+\frac{1}{2}} + p^+_{j,k+\frac{1}{2}}\right).
\end{aligned}$$

Remark 3.5 As in the 1-D case, the 2-D new LDCU scheme results in a system of time-dependent ODEs (3.27), which has to be solved using a stable and sufficiently accurate ODE solver. In all of the numerical experiments reported in §4.2, we have used the three stage third-order SSP Runge–Kutta method; see, e.g., [7, 8]. The time steps have been selected adaptively using the following CFL condition:

$$\Delta t \le \frac{1}{2}\min\left\{\frac{\Delta x}{a_{\max}}, \frac{\Delta y}{b_{\max}}\right\},$$

where

$$a_{\max} := \max_{j,k}\left[\max\left\{a^+_{j+\frac{1}{2},k}, -a^-_{j+\frac{1}{2},k}\right\}\right], \quad b_{\max} := \max_{j,k}\left[\max\left\{b^+_{j,k+\frac{1}{2}}, -b^-_{j,k+\frac{1}{2}}\right\}\right].$$

4 Numerical Examples

In this section, we present both 1-D and 2-D numerical examples. Our main goal is to demonstrate that the new LDCU schemes contain substantially smaller amount of the numerical

Table 1 Example 1: The L^1-errors and experimental convergence rates for the density ρ, momentum ρu, and total energy E

Δx	ρ		ρu		E	
	Error	Rate	Error	Rate	Error	Rate
1/200	3.93e−05	2.05	1.05e−04	2.06	5.02e−04	2.06
1/400	9.74e−06	2.03	2.57e−05	2.04	1.24e−04	2.04
1/800	2.18e−06	2.09	5.76e−06	2.09	2.76e−05	2.10
1/1600	5.23e−07	2.08	1.37e−06	2.08	6.59e−06	2.08
1/3200	1.27e−07	2.06	3.33e−07	2.07	1.60e−06	2.07

dissipation compared with the old CU schemes from [10], which we will refer to as the CU schemes. We will show that despite having less numerical dissipation, the LDCU schemes produce non-oscillatory results and also achieve higher resolution than the CU ones. The advantages will be especially pronounced when the numerical solutions contain contact waves, shear layers, vortices as well as small-scale 2-D structures.

In Examples 1–10, we take $\gamma = 1.4$, while in Example 11, we take $\gamma = 5/3$. In all of the examples, we have used the CFL number 0.475, the generalized minmod parameter $\theta = 1.3$, and the small parameter $\varepsilon = 10^{-12}$.

4.1 One-Dimensional Examples

Example 1 (1-D Accuracy Test) In the first example taken from [5], we consider the problem subject to the following smooth initial data:

$$u(x,0) = \sin\left(\frac{\pi x}{5} + \frac{\pi}{4}\right), \quad \rho(x,0) = \left[\frac{\gamma-1}{2\sqrt{\gamma}}\left(u(x,0)+10\right)\right]^{\frac{2}{\gamma-1}}, \quad p(x,0) = \rho^{\gamma}(x,0).$$

We impose the periodic boundary conditions and compute the numerical solution on the computational domain $[0, 10]$ until the final time $t = 0.1$ using the LDCU scheme on a sequence of uniform meshes with $\Delta x = 1/50$, 1/100, 1/200, 1/400, 1/800, 1/1600, and 1/3200.

We then compute the L^1-errors and estimate the experimental convergence rates using the following Runge formulae, which are based on the solutions computed on the three consecutive uniform grids with the mesh sizes Δx, $2\Delta x$, and $4\Delta x$ and denoted by $(\cdot)^{\Delta x}$, $(\cdot)^{2\Delta x}$, and $(\cdot)^{4\Delta x}$, respectively:

$$\text{Error}(\Delta x) \approx \frac{\delta_{12}^2}{|\delta_{12}-\delta_{24}|}, \quad \text{Rate}(\Delta x) \approx \log_2\left(\frac{\delta_{24}}{\delta_{12}}\right).$$

Here, $\delta_{12} := ||(\cdot)^{\Delta x} - (\cdot)^{2\Delta x}||_{L^1}$ and $\delta_{24} := ||(\cdot)^{2\Delta x} - (\cdot)^{4\Delta x}||_{L^1}$. The computed L^1-errors and corresponding convergence rates for the density, momentum, and total energy are reported in Table 1, where one can clearly see that the second order of accuracy is achieved.

Example 2 (Moving Contact Wave) In the second example, we consider the following initial conditions:

$$(\rho(x,0), u(x,0), p(x,0)) = \begin{cases} (1.4, 0.1, 1), & x < 0.3, \\ (1.0, 0.1, 1), & x > 0.3, \end{cases}$$

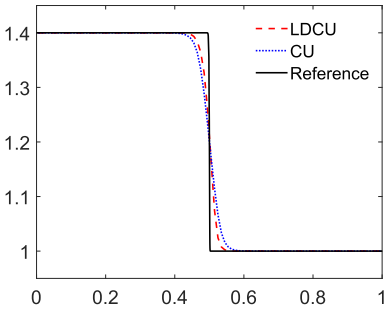

Fig. 4 Example 2: Density (ρ) computed by the LDCU and CU schemes

prescribed in the computational domain [0, 1] subject to the free boundary conditions. We compute the solution which contains an isolated moving contact discontinuity, until the final time $t = 2$ by the LDCU and CU schemes on a uniform mesh with $\Delta x = 1/100$. The obtained densities are presented in Fig. 4, where one can see that the LDCU scheme clearly outperforms the CU one.

We also measure the CPU times consumed by the LDCU and CU schemes on a uniform mesh with $\Delta x = 1/2000$. They are about 24.60 s for the CU scheme and 21.54 s for the LDCU schemea (the computations have been carried out on the Lenovo ThinkPad T480 laptop). This shows that the computational cost is reduced by about 12% when the LDCU scheme is used, which gives an additional evidence of the advantage of the proposed LDCU scheme over its predecessor. We would like to stress that the only difference between the two studied schemes is in the "built-in" anti-diffusion terms, which are clearly more computationally expensive in the CU scheme.

Example 3 (Stationary Contact Wave and Traveling Shock and Rarefaction) In this example taken from [10], we consider the following Riemann initial data:

$$(\rho(x,0), u(x,0), p(x,0)) = \begin{cases} (1, -19.59745, 1000), & x < 0.8, \\ (1, -19.59745, 0.01), & x > 0.8, \end{cases}$$

prescribed in the computational domain [0, 1] subject to the free boundary conditions. The exact solution of this initial-value problem consists of a stationary contact wave, a traveling shock, and a traveling rarefaction wave. We compute the LDCU and CU solutions until the final time $t = 0.012$ on a uniform mesh with $\Delta x = 1/200$. The obtained densities together with the reference solution computed using the LDCU scheme on a much finer uniform mesh with $\Delta x = 1/10000$ are plotted in Fig. 5. As one can see, the LDCU scheme achieves a much sharper resolution around the contact discontinuity area despite producing a small overshoot.

Example 4 ("Shock-Bubble" Interaction) In the fourth example, we consider the initial data that correspond to a left-moving shock, initially located at $x = 0.75$, and a "bubble" of radius 0.25, initially located at the origin:

$$(\rho(x,0), u(x,0), p(x,0)) = \begin{cases} (13.1538, 0, 1), & |x| < 0.25, \\ (1.3333, -0.3535, 1.5), & x > 0.75, \\ (1, 0, 1), & \text{otherwise}. \end{cases}$$

These data are prescribed in the computational domain $[-1, 1]$ subject to the solid wall boundary conditions on the left and free boundary conditions on the right.

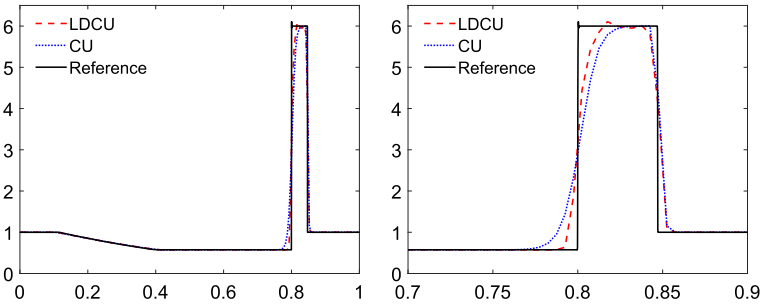

Fig. 5 Example 3: Density (ρ) computed by the LDCU and CU schemes (left) and zoom at the contact discontinuity area (right)

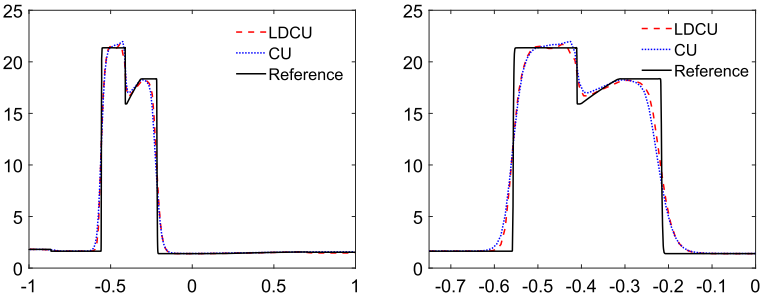

Fig. 6 Example 4: Density (ρ) computed by the LDCU and CU schemes (left) and zoom at $[-0.75, 0]$ (right)

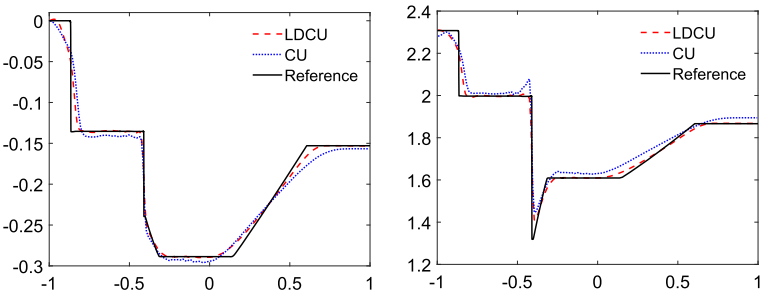

Fig. 7 Example 4: Velocity (u) (left) and pressure (p) (right) computed by the LDCU and CU schemes

We compute the solutions by the LDCU and CU schemes until the final time $t = 3$ on a uniform mesh with $\Delta x = 1/100$ and obtain the reference solution using the LDCU scheme on a much finer mesh with $\Delta x = 1/4000$. The obtained densities are plotted in Fig. 6, where one can see that the LDCU scheme achieves a slightly better resolution. We also plot the computed velocities and pressure (see Fig. 7), where the advantage of the LDCU scheme is more pronounced. This clearly indicates that the LDCU scheme outperforms the CU one.

Table 2 Example 5: The L^1-errors and experimental convergence rates for the density ρ, momenta ρu and ρv, and total energy E

$\Delta x = \Delta y$	ρ		ρu		ρv		E	
	Error	Rate	Error	Rate	Error	Rate	Error	Rate
1/100	6.59e−04	–	6.59e−04	–	4.62e−04	–	4.91e−04	–
1/200	1.54e−04	2.10	1.54e−04	2.10	1.08e−04	2.10	1.15e−04	2.10
1/400	3.68e−05	2.06	3.68e−05	2.06	2.58e−05	2.06	2.74e−05	2.06
1/800	8.11e−06	2.18	8.11e−06	2.18	5.67e−06	2.18	6.04e−06	2.18

4.2 Two-Dimensional Examples

Example 5 (2-D Accuracy Test) In the first 2-D example taken from [14], we consider the 2-D Euler equations of gas dynamics subject to the following periodic initial conditions:

$$\rho(x, y, 0) = 1 + \frac{1}{2}\sin(\pi(x + y)), \quad u(x, y, 0) \equiv 1, \quad v(x, y, 0) \equiv -0.7, \quad p(x, y, 0) \equiv 1.$$

The exact solution of this initial value problem is given by

$$\rho(x, y, t) = 1 + \tfrac{1}{2}\sin(\pi(x + y - 0.3t)),$$
$$u(x, y, t) \equiv 1, \quad v(x, y, t) \equiv -0.7, \quad p(x, y, t) \equiv 1.$$

We first compute the numerical solution on the computational domain $[-1, 1] \times [-1, 1]$ until the final time $t = 0.1$ using the LDCU scheme on a sequence of uniform meshes with $\Delta x = \Delta y = 1/50$, 1/100, 1/200, and 1/400. We then measure the L^1-errors and compute the corresponding experimental convergence rates. The obtained results presented in Table 2 confirm that the second order of accuracy is achieved by the LDCU scheme.

Example 6 (Moving Contact Wave) In the second 2-D example which was proposed in [11], we consider an isolated moving contact wave in the computational domain $\Omega = [-0.2, 0.2] \times [0, 0.8]$ with the following initial data:

$$\big(\rho(x, y, 0), u(x, y, 0), v(x, y, 0), p(x, y, 0)\big) = \begin{cases} (1.4, 0, 0.2, 1), & (x, y) \in D, \\ (1.0, 0, 0.2, 1), & \text{otherwise}, \end{cases}$$

where D is the domain consisting of the points $(x, y) \in \Omega$ satisfying the following conditions:

$$\{-0.1 < x < 0.1,\ 0 < y < 0.02\} \bigcup \{-0.02 < x < 0.02,\ 0.02 < y < 0.1\} \bigcup$$
$$\left\{(x + 0.02)^2 + (y - 0.02)^2 < 0.08^2\right\} \bigcup \left\{(x - 0.02)^2 + (y - 0.02)^2 < 0.08^2\right\}.$$

We apply free boundary conditions and compute the solution until the final time $t = 2$ on the uniform mesh with $\Delta x = \Delta y = 1/250$. The densities computed by the LDCU and CU schemes are plotted in Fig. 8. As one can see, the solution computed by the CU scheme is much more smeared due to a substantially larger amount of dissipation present in the CU scheme compared with the LDCU scheme. This is especially pronounced in the x-direction, in which the LDCU solution maintains almost perfect jump discontinuities.

We also measure the CPU times consumed by the LDCU and CU schemes. They are about 145.69 s for the CU scheme and 111.77 s for the LDCU scheme (the computations have been

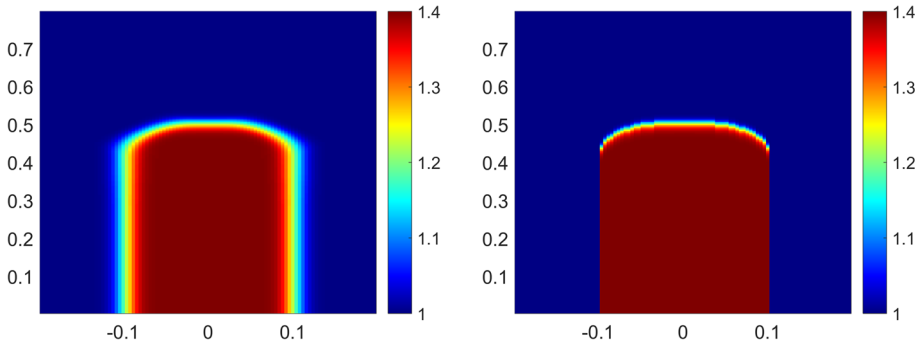

Fig. 8 Example 6: Density (ρ) computed by the CU (left) and LDCU (right) schemes

carried out on the Lenovo ThinkPad T480 laptop). This shows that the computational cost is reduced by about 23% when the LDCU scheme is used, which gives an additional evidence of the advantage of the proposed LDCU scheme over its predecessor. Notice that in the 2-D case, the difference in the consumed CPU times is bigger than in the 1-D case since the due to the "built-in" anti-diffusion term in the 2-D CU scheme is increasingly computational expensive.

Example 7 (Two-Dimensional Riemann Problem) In this example, we consider Configuration 3 of the 2-D Riemann problems from [16]; also see [27, 28, 35]. The initial conditions,

$$(\rho(x,y,0),u(x,y,0),v(x,y,0),p(x,y,0)) = \begin{cases} (1.5,0,0,1.5), & x>1,\ y>1,\\ (0.5323,1.206,0,0.3), & x<1,\ y>1,\\ (0.138,1.206,1.206,0.029), & x<1,\ y<1,\\ (0.5323,0,1.206,0.3), & x>1,\ y<1, \end{cases}$$

are prescribed on the domain $[0,1.2]\times[0,1.2]$ subject to free boundary conditions. We compute the solution until the final time $t=1$ on a uniform mesh with $\Delta x=\Delta y=0.0012$. The densities computed by the LDCU and CU schemes are presented in Fig. 9. As one can observe, both schemes maintain the diagonal symmetry of the jet. However, one can clearly see that the LDCU scheme captures a sideband instability of the jet in the zones of strong along-jet velocity shear and the instability along the jet's neck with a much higher resolution. One may also notice the presence of the certain numerical oscillation in the LDCU solution, which is expected to occur when the numerical dissipation is reduced.

Example 8 (Explosion Problem) We now consider the explosion problem taken from [22]. The initial conditions,

$$(\rho(x,y,0),u(x,y,0),v(x,y,0),p(x,y,0)) = \begin{cases} (1,0,0,1), & x^2+y^2<0.16,\\ (0.125,0,0,0.1), & \text{otherwise}, \end{cases}$$

are prescribed in the computational domain $[0,1.5]\times[0,1.5]$ subject to the solid wall boundary conditions at $x=0$ and $y=0$ and free boundary conditions at $x=1.5$ and $y=1.5$. We compute the solution until the final time $t=3.2$ by the LDCU and CU schemes on a uniform mesh with $\Delta x=\Delta y=3/800$. The obtained densities are presented in Fig. 10.

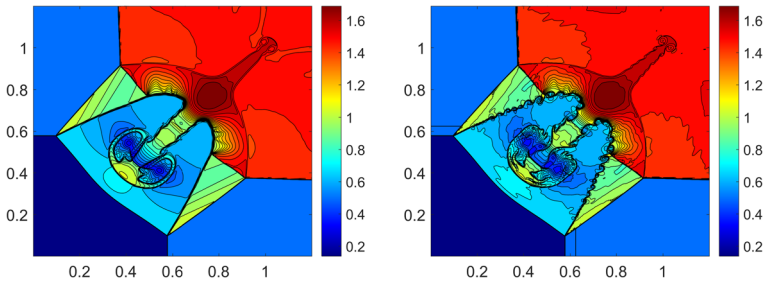

Fig. 9 Example 7: Density (ρ) computed by the CU (left) and LDCU (right) schemes

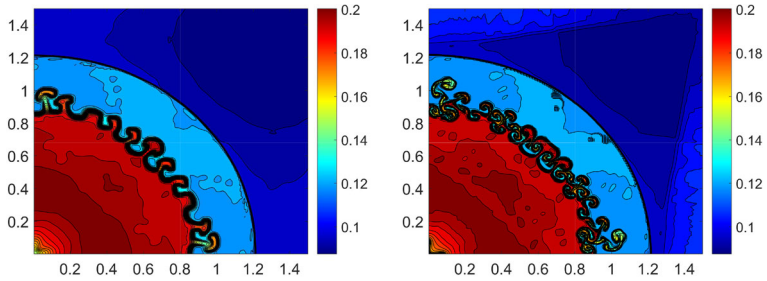

Fig. 10 Example 8: Density (ρ) computed by the CU (left) and LDCU (right) schemes

The advantage of the LDCU scheme can be seen in the fact that the contact wave captured by the LDCU scheme is much "curlier". This demonstrates that the amount of the numerical dissipation present in the LDCU scheme is substantially smaller compared with the CU one.

Example 9 (Implosion Problem) In this example, we test the implosion problem also taken from [22]. The initial conditions,

$$(\rho(x,y,0),u(x,y,0),v(x,y,0),p(x,y,0)) = \begin{cases} (0.125,0,0,0.14), & |x|+|y|<0.15, \\ (1,0,0,1), & \text{otherwise}, \end{cases}$$

are prescribed in the computational domain $[0,0.3]\times[0,0.3]$ subject to the solid wall boundary conditions. We compute the solution until the final time $t = 2.5$ by the LDCU and CU schemes on a uniform mesh with $\Delta x = \Delta y = 1/2000$. The obtained densities are presented in Fig. 11. As one can observe, the jet generated by the LDCU scheme propagates to a much larger extent than the jet produced by the CU scheme. This once again demonstrates that the LDCU scheme has a much smaller amount of numerical dissipation compared with the CU one.

Example 10 (Kelvin–Helmholtz (KH) Instability) In this example, we consider the KH instability, which occurs in many natural phenomena: the so-called "wind-over-water" and "clear air turbulence" instabilities. The KH instability is triggered by shear flows, often also involving fluids with different densities, and grows exponentially until the primary billows break, subsequently leading to a two-phase turbulence. In order to show better capabilities of the LDCU scheme in capturing small scale turbulent structures, we take the following initial

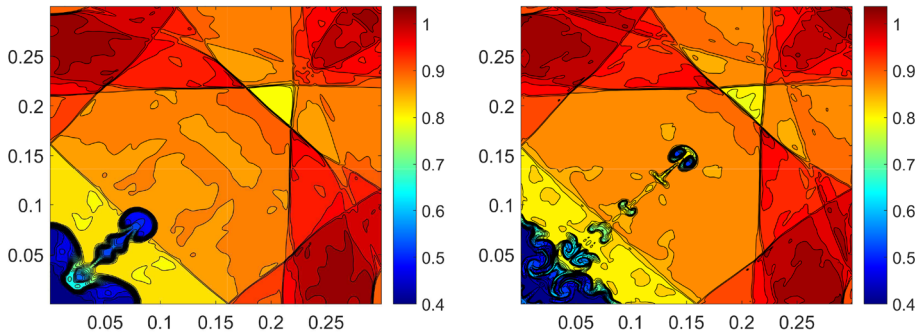

Fig. 11 Example 9: Density (ρ) computed by the CU (left) and LDCU (right) schemes

conditions studied in [6, 11, 25]:

$$(\rho(x,y,0),u(x,y,0)) = \begin{cases} (1,-0.5+0.5e^{(y+0.25)/L}), & y\in[-0.5,-0.25),\\ (2,0.5-0.5e^{(-y-0.25)/L}), & y\in[-0.25,0),\\ (2,0.5-0.5e^{(y-0.25)/L}), & y\in[0,0.25),\\ (1,-0.5+0.5e^{(0.25-y)/L}), & y\in[0.25,0.5], \end{cases}$$

$$v(x,y,0)=0.01\sin(4\pi x),\quad p(x,y,0)\equiv 1.5,$$

where L is a smoothing parameter taken to be 0.00625, which corresponds to a thin shear interface with a periodic vertical velocity field v. We use the computational domain is $[-0.5,0.5]\times[-0.5,0.5]$ and set the periodic boundary conditions.

We compute the solution until the final time $t=4$ by the LDCU and CU schemes on a uniform mesh with $\Delta x=\Delta y=1/1024$. The density snapshots at times $t=1$, 2.5, and 4 are presented in Fig. 12. As one can see, at time $t=1$, the vortex sheets formed by the CU scheme are quite smeared by the numerical dissipation, while in the LDCU scheme these vortex sheets are much more pronounced. At the later times $t=2.5$ and 4, one can observe much more complicated vortices and the two-phase turbulence in the "swirls" in the densities computed by the LDCU scheme. This indicates that the LDCU scheme can capture the KH instabilities much better than the CU scheme.

Example 11 (Raleigh–Taylor (RT) Instability) In the final example, we investigate the RT instability, which naturally occurs when a layer of heavier fluid is placed on top of a layer of lighter fluid. In order to study the RT instability, we solve the following 2-D Euler equations with gravitation acting upward in the y-direction:

$$\begin{aligned} &\rho_t+(\rho u)_x+(\rho v)_y=0,\\ &(\rho u)_t+(\rho u^2+p)_x+(\rho uv)_y=0,\\ &(\rho v)_t+(\rho uv)_x+(\rho v^2+p)_y=\rho,\\ &E_t+(u(E+p))_x+(v(E+p))_y=\rho v. \end{aligned} \tag{4.1}$$

In the performed simulations, the cell averages of the source terms in (4.1) have been approximated in a straightforward way, namely, using a midpoint rule.

We use the setting from [29] and consider the following initial conditions:

$$(\rho(x,y,0),u(x,y,0),v(x,y,0),p(x,y,0))$$

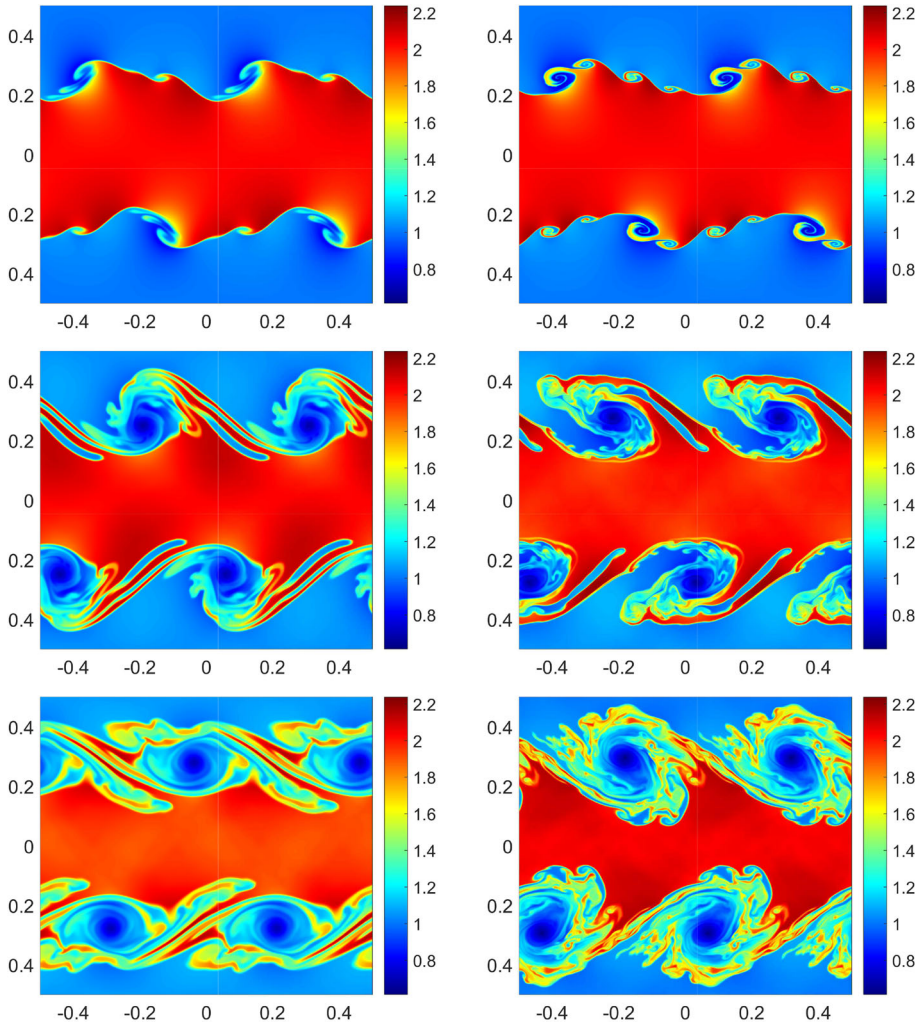

Fig. 12 Example 10: Density (ρ) computed by the CU (left column) and LDCU (right column) schemes at times $t = 1$ (top row), $t = 2.5$ (middle row), and $t = 4$ (bottom row)

$$= \begin{cases} (2,\, 0,\, -0.025c\cos(8\pi x),\, 2y+1), & y < 0.5, \\ (1,\, 0,\, -0.025c\cos(8\pi x),\, y+1.5), & \text{otherwise}, \end{cases}$$

where $c = \sqrt{\gamma p/\rho}$ is the speed of sound. The computational domain is $[0,\, 1/4] \times [0,\, 1]$. We impose the solid wall boundary conditions at $x = 0$ and $x = 1/4$ and the following Dirichlet boundary conditions at the top and bottom boundaries:

$$(\rho, u, v, p)\Big|_{y=1} \equiv (1, 0, 0, 2.5) \quad \text{and} \quad (\rho, u, v, p)\Big|_{y=0} \equiv (2, 0, 0, 1).$$

We compute the solution by the LDCU and CU schemes until the final time $t = 2.95$ on a uniform mesh with $\Delta x = \Delta y = 1/1024$ and plot the obtained densities in Fig. 13. As one can see, the LDCU scheme captures much more complicated structures than the CU one,

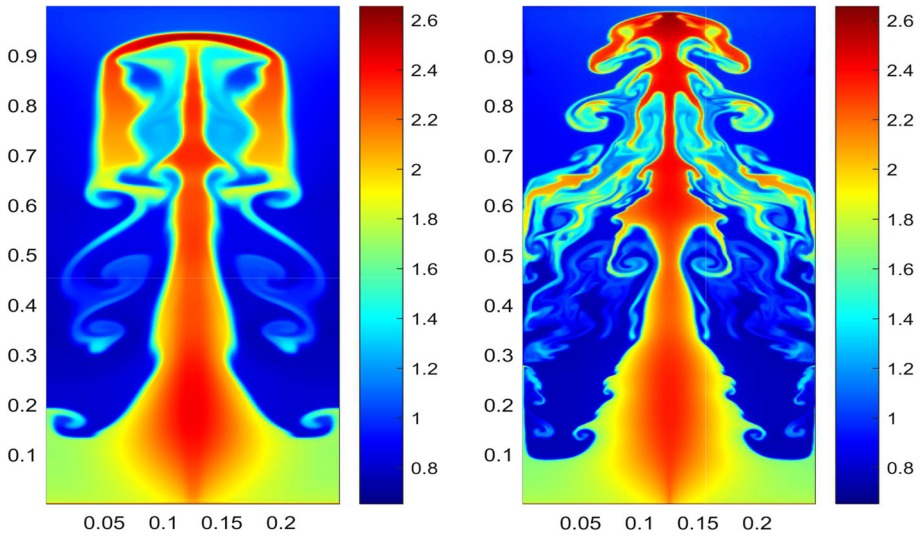

Fig. 13 Example 11: Density (ρ) computed by the CU (left) and LDCU (right) schemes

which clearly indicates that the amount of numerical dissipation in the LDCU scheme is substantially smaller.

5 Conclusion

In this paper, we have developed a new second-order semi-discrete low-dissipation central-upwind (LDCU) scheme. Compared with the central-upwind (CU) scheme from [10], the LDCU scheme contains substantially smaller amount of numerical dissipation and yet leads to stable solutions, which are essentially non-oscillatory, that is, when the oscillations are developed, they are small and controllable. In order to achieve this goal, we modify the projection step in the construction of the CU schemes. The new projection step is based on a subcell resolution and it is designed to better approximate contact waves, whose resolution are typically strongly affected by excessive numerical dissipation present in many non-oscillatory central and CU Godunov-type schemes.

We have developed the LDCU schemes for 1-D and 2-D Euler equations of gas dynamics and tested the proposed schemes on a variety of numerical examples. In the 1-D examples, we have demonstrated that the LDCU schemes clearly outperforms the CU scheme from [10], especially when capturing contact waves. In the 2-D examples, we have illustrated that the LDCU scheme can handle not only the contact waves, but also the small-scale structures and a variety of instabilities with a much higher resolution compared with the 2-D CU scheme from [10]. The performed numerical experiments indicate that the amount of numerical dissipation present in the LDCU schemes is substantially smaller than in the CU schemes from [10].

The proposed LDCU numerical flux can be used as a basis for the derivation of higher-order schemes within, for example, the weighted essentially non-oscillatory (WENO) framework;

see, e.g., the recent review papers [30, 31] and references therein. Development of such schemes is a subject of our future work.

Funding The work of A. Kurganov was supported in part by NSFC Grants 12171226 and 12111530004, and by the fund of the Guangdong Provincial Key Laboratory of Computational Science and Material Design (No. 2019B030301001).

Data and Software Availability The data that support the findings of this study and FORTRAN codes developed by the authors and used to obtain all of the presented numerical results are available from the corresponding author upon reasonable request.

Declarations

Conflict of interest On behalf of all authors, the corresponding author states that there is no conflict of interest.

References

1. Arminjon, P., St-Cyr, A., Madrane, A.: New two- and three- dimensional non-oscillatory central finite volume methods on staggered Cartesian grids. Appl. Numer. Math. **40**, 367–390 (2002)
2. Arminjon, P., Viallon, M.-C., Madrane, A.: A finite volume extension of the Lax–Friedrichs and Nessyahu–Tadmor schemes for conservation laws on unstructured grids. Int. J. Comput. Fluid Dyn. **9**, 1–22 (1997)
3. Ben-Artzi, M., Falcovitz, J.: Generalized Riemann Problems in Computational Fluid Dynamics. Cambridge Monographs on Applied and Computational Mathematics, vol. 11. Cambridge University Press, Cambridge (2003)
4. Bianco, F., Puppo, G., Russo, G.: High order central schemes for hyperbolic systems of conservation laws. SIAM J. Sci. Comput. **21**, 294–322 (1999)
5. Chertock, A., Chu, S., Herty, M., Kurganov, A., Lukáčová-Medviďová, M.: Local characteristic decomposition based central-upwind scheme. J. Comput. Phys., **473** (2023). Paper No. 111718, 24 pp
6. Fjordholm, U.S., Mishra, S., Tadmor, E.: On the computation of measure-valued solutions. Acta Numer. **25**, 567–679 (2016)
7. Gottlieb, S., Ketcheson, D., Shu, C.-W.: Strong Stability Preserving Runge–Kutta and Multistep time Discretizations. World Scientific Publishing Co Pte. Ltd., Hackensack, NJ (2011)
8. Gottlieb, S., Shu, C.-W., Tadmor, E.: Strong stability-preserving high-order time discretization methods. SIAM Rev. **43**, 89–112 (2001)
9. Jiang, G.-S., Tadmor, E.: Nonoscillatory central schemes for multidimensional hyperbolic conservation laws, SIAM J. Sci. Comput. **19**, pp. 1892–1917 (electronic) (1998)
10. Kurganov, A., Lin, C.-T.: On the reduction of numerical dissipation in central-upwind schemes. Commun. Comput. Phys. **2**, 141–163 (2007)
11. Kurganov, A., Liu, Y., Zeitlin, V.: Numerical dissipation switch for two-dimensional central-upwind schemes. ESAIM Math. Model. Numer. Anal. **55**, 713–734 (2021)
12. Kurganov, A., Noelle, S., Petrova, G.: Semidiscrete central-upwind schemes for hyperbolic conservation laws and Hamilton–Jacobi equations. SIAM J. Sci. Comput. **23**, 707–740 (2001)
13. Kurganov, A., Petrova, G.: A third-order semi-discrete genuinely multidimensional central scheme for hyperbolic conservation laws and related problems. Numer. Math. **88**, 683–729 (2001)
14. Kurganov, A., Prugger, M., Wu, T.: Second-order fully discrete central-upwind scheme for two-dimensional hyperbolic systems of conservation laws. SIAM J. Sci. Comput. **39**, A947–A965 (2017)
15. Kurganov, A., Tadmor, E.: New high-resolution central schemes for nonlinear conservation laws and convection-diffusion equations. J. Comput. Phys. **160**, 241–282 (2000)
16. Kurganov, A., Tadmor, E.: Solution of two-dimensional Riemann problems for gas dynamics without Riemann problem solvers. Numer. Methods Partial Differ. Equ. **18**, 584–608 (2002)
17. LeVeque, R.J.: Finite Volume Methods for Hyperbolic Problems, Cambridge Texts in Applied Mathematics, Cambridge University Press, Cambridge (2002)
18. Levy, D., Puppo, G., Russo, G.: Central WENO schemes for hyperbolic systems of conservation laws. Modél. Math. Anal. Numér. **33**, 547–571 (1999)
19. Levy, D., Puppo, G., Russo, G.: Compact central WENO schemes for multidimensional conservation laws. SIAM J. Sci. Comput., **22**, pp. 656–672 (electronic) (2000)

20. Levy, D., Puppo, G., Russo, G.: A fourth-order central WENO scheme for multidimension hyperbolic systems of conservation laws. SIAM J. Sci. Comput. **24**, 480–506 (2002)
21. Lie, K.-A., Noelle, S.: On the artificial compression method for second-order nonoscillatory central difference schemes for systems of conservation laws. SIAM J. Sci. Comput. **24**, 1157–1174 (2003)
22. Liska, R., Wendroff, B.: Comparison of several difference schemes on 1D and 2D test problems for the Euler equations. SIAM J. Sci. Comput. **25**, 995–1017 (2003)
23. Liu, X.-D., Tadmor, E.: Third order nonoscillatory central schemes for hyperbolic conservation laws. Numer. Math. **79**, 397–425 (1998)
24. Nessyahu, H., Tadmor, E.: Nonoscillatory central differencing for hyperbolic conservation laws. J. Comput. Phys. **87**, 408–463 (1990)
25. Panuelos, J., Wadsley, J., Kevlahan, N.: Low shear diffusion central schemes for particle methods, J. Comput. Phys., **414**. Paper No. 109454, 23 pp (2020)
26. Qiu, J., Shu, C.-W.: On the construction, comparison, and local characteristic decomposition for high-order central WENO schemes. J. Comput. Phys. **183**, 187–209 (2002)
27. Schulz-Rinne, C.W.: Classification of the Riemann problem for two-dimensional gas dynamics. SIAM J. Math. Anal. **24**, 76–88 (1993)
28. Schulz-Rinne, C.W., Collins, J.P., Glaz, H.M.: Numerical solution of the Riemann problem for two-dimensional gas dynamics. SIAM J. Sci. Comput. **14**, 1394–1414 (1993)
29. Shi, J., Zhang, Y.-T., Shu, C.-W.: Resolution of high order WENO schemes for complicated flow structures. J. Comput. Phys. **186**, 690–696 (2003)
30. Shu, C.-W.: High order weighted essentially nonoscillatory schemes for convection dominated problems. SIAM Rev. **51**, 82–126 (2009)
31. Shu, C.-W.: Essentially non-oscillatory and weighted essentially non-oscillatory schemes. Acta Numer. **29**, 701–762 (2020)
32. Sweby, P.K.: High resolution schemes using flux limiters for hyperbolic conservation laws. SIAM J. Numer. Anal. **21**, 995–1011 (1984)
33. Toro, E.F.: Riemann Solvers and Numerical Methods for Fluid Dynamics: A Practical Introduction, third ed. Springer, Berlin (2009)
34. van Leer, B.: Towards the ultimate conservative difference scheme. V. A second-order sequel to Godunov's method. J. Comput. Phys., **32**, pp. 101–136 (1979)
35. Zheng, Y.: Systems of Conservation Laws: Two-Dimensional Riemann Problems, Progress in Nonlinear Differential Equations and their Applications, 38. Birkhäuser Boston Inc, Boston, MA (2001)